

Review

# Recent Progress in the Application of Palladium Nanoparticles: A Review

Marwa Alaqarbeh <sup>1</sup>, Syed Farooq Adil <sup>2,\*</sup>, Tamara Ghrear <sup>3</sup>, Mujeeb Khan <sup>2</sup>, Mohammed Bouachrine <sup>4,5</sup> and Abdulrahman Al-Warthan <sup>2,\*</sup>

<sup>1</sup> Basic Science Department, Prince Al Hussein Bin Abdullah II Academy for Civil Protection, Al-Balqa Applied University, Al-Salt 19117, Jordan; marwaqarbh@hotmail.com

<sup>2</sup> Department of Chemistry, College of Science, King Saud University, P.O. Box 2455, Riyadh 11451, Saudi Arabia; kmujeeb@ksu.edu.sa

<sup>3</sup> Department of Basic Sciences, Faculty Arts and Educational Sciences, Middle East University, Amman 11610, Jordan; tghrear@meu.edu.jo

<sup>4</sup> Molecular Chemistry and Natural Substances Laboratory, Faculty of Science, Moulay Ismail University of Meknes, Meknes 50050, Morocco; m.bouachrine@umi.ac.ma

<sup>5</sup> Biotechnology, Bioresources and Bioinformatics Laboratory, Higher School of Technology-Khenifra, University of Sultan My Slimane, Khenifra 54000, Morocco

\* Correspondence: sfadil@ksu.edu.sa (S.F.A.); awarthan@ksu.edu.sa (A.A.-W.)

**Abstract:** Palladium (Pd), a noble metal, has unique properties for C-C bond formation in reactions such as the Suzuki and Heck reactions. Besides Pd-based complexes, Pd NPs have also attracted significant attention for applications such as fuel cells, hydrogen storage, and sensors for gases such as H<sub>2</sub> and non-enzymatic glucose, including catalysis. Additionally, Pd NPs are catalysts in environmental treatment to abstract organic and heavy-metal pollutants such as Cr (VI) by converting them to Cr(III). In terms of biological activity, Pd NPs were found to be active against *Staphylococcus aureus* and *Escherichia coli*, where 99.99% of bacteria were destroyed, while PVP-Pd NPs displayed anticancer activity against human breast cancer MCF7. Hence, in this review, we attempted to cover recent progress in the various applications of Pd NPs with emphasis on their application as sensors and catalysts for energy-related and other applications.

**Keywords:** palladium; nanoparticles; sensors; catalysis; environmental remediation; antibacterial; anticancer



**Citation:** Alaqarbeh, M.; Adil, S.F.; Ghrear, T.; Khan, M.; Bouachrine, M.; Al-Warthan, A. Recent Progress in the Application of Palladium Nanoparticles: A Review. *Catalysts* **2023**, *13*, 1343. <https://doi.org/10.3390/catal13101343>

Academic Editor: Pitchaimani Veerakumar

Received: 30 August 2023

Revised: 26 September 2023

Accepted: 28 September 2023

Published: 4 October 2023



**Copyright:** © 2023 by the authors. Licensee MDPI, Basel, Switzerland. This article is an open access article distributed under the terms and conditions of the Creative Commons Attribution (CC BY) license (<https://creativecommons.org/licenses/by/4.0/>).

## 1. Introduction

Recently, scientific research and industrial applications have been interested in transition metal nanoparticles (TMNPs) due to their unique optical, electronic, and catalytic properties [1–9]. Notably, noble metal NPs that include palladium (Pd) and ruthenium (Ru), rhenium (Re), rhodium (Rh), silver (Ag), osmium (Os), iridium (Ir), platinum (Pt), and gold (Au) have received a lot of attention in vast areas like sensors, energy conversion, biomedical treatment, and catalysis [10–12]. Palladium (Pd), which is the same group as platinum, possesses the unequalled electronic ground-state structure of Pd (4d<sup>10</sup>5s<sup>0</sup>) and the square-planar geometry of Pd(II) complexes with further axial positioned coordination sites, which can be expanded by employing numerous ligands, giving Pd distinctive properties for C-C bond formation and C-O bond cleavage [13].

Apart from this, palladium (Pd) NPs have received massive attention due to their exceptional properties that give them high catalytic activity and the ability to adsorb hydrogen at low temperatures. [14]. Additionally, they are also used in fuel cells, photothermal therapy, anticancer treatment, hydrogen storage, antibacterial applications, and sensors [15]. In addition, palladium NPs (Pd NPs) have been synthesized with high surface area and active sites [16].

In synthesizing Pd-based nanomaterials, one has to consider many points: (i) control of size and shape to reach an optimum of chemically active sites; (ii) control of high-index factors for enhanced catalytic activity; (iii) development of bi- and tri-metallic compositions and architectures to improve stability and activity; (iv) foundation of essential correlations between composition, structure, and reactivity of Pd nanomaterials to prepare highly competent catalysts; (v) finding new substrate materials with high chemical, conductivity, and mechanical stability, and also large surface area; and (vi) permitting the uniform distribution of Pd-based catalysts on support materials to enhance efficiency [17].

In this regard, Pd NPs were synthesized by three types of method: a chemical method [18], a physical method [19], and a biological method [20], but on the industrial scale, the physical method and chemical method were of interest. Physical methods included magnetron sputtering [21], physical vapor deposition [22], and laser ablation [23]. However, the synthesized physical method required expensive equipment and energy-intensive processes, including maintaining high pressure and high temperatures [24]. On the other hand, the chemical method depended on the chemical reduction of metal ions to zero-valent metal atoms and their nucleation to form NPs [25]. These methods include supercritical fluid nucleation [26], electrochemical deposition [27], sonochemical preparation [28], and wet chemical methods [29] such as the sol-gel method or reduction by alcohols or other reductants. The disadvantages of chemical synthesis methods involve reducing or stabilizing agents, hazardous solvents, or producing toxic side products [30]. However, biological methods, such as biogenic methods, are more interesting in pharmaceutical and biomedical applications due to the principle of providing simple, rapid, potentially more environmentally friendly, and cost-effective methods. Furthermore, the biogenic method has displayed control over physical properties of NPs such as size and shape [31]. Notably, the properties and performance of efficient catalysts depend on the shape and size of the nanomaterial; models for the shape-selective synthesis of Pd nanostructures were published, such as Pd nanowires (Pd NWs), Pd broccolis (Pd NBRs), and Pd nanorods (Pd NRs) [32].

On the other hand, Pd NPs tend to agglomerate, leading to a decrease in the surface area. To overcome this problem, Pd NPs should be immobilized on the surface of a solid support such as metal oxide [33], silica [34], polystyrene [35], activated carbon [36], or carbon nanotubes [37]. A solid support helps to increase the activity of the catalyst by preventing the aggregation of Pd NPs, enhancing the stability and simplifying the recovery of the catalyst after the reaction, thus decreasing the cost and the chemicals used [38]. In addition, there are different ways to improve Pd NPs, such as bimetallic catalysts. Pd-based bimetallic catalysts, for instance, Pd-Cu, Pd-Ru, Pd-Ni, and Pd-Co, have shown high performance in catalytic activity and selectivity for goal products due to new properties of electronic and chemical structure [39].

This review aims to compile literature about palladium metallic nanoparticles and their applications in various areas such as sensors, catalysis, and energy, with an aim to put forward prospects for future research directions.

## 2. Sensing Applications

### 2.1. Palladium-Based Nanocomposites for Sensing Applications

Metallic nanostructures have gained significant interest for a variety of applications including sensing, due to their diverse morphologies and sizes; unique electronic, plasmonic, and optical properties; and their outstanding chemical stability and varied oxidation states [40,41]. In particular, nanostructures involving gold-, silver-, iron-, palladium-, and platinum-based hybrid nanomaterials typically offer tremendous possibilities in a variety of sensing applications [42–44]. Among these metallic nanostructures, noble palladium nanoparticles offer superb physicochemical properties, like strong chemical and thermal stability; excellent electronic, plasmonic and optical properties; and high catalytic activity. In addition to this, palladium is less expensive, readily available, and can be easily synthesized in different morphologies and sizes using simple synthetic approaches [45–48].

Palladium nanoparticles can be easily combined or coated with different types of functional materials or ligands to fabricate a variety of advanced functional materials with desirable properties [49–51]. Palladium nanoparticles have gained particularly significant recognition in the field of catalysis, which has been utilized to create different types of catalysts for several organic transformations including C-C bond formation [52–54]. Apart from this, palladium-based nanostructures have also been extensively applied in hydrogen storage, fuel cells, and sensors [55–57]. Palladium exhibits the unique capability to reversibly absorb gases, particularly hydrogen, in large quantities under ambient conditions, which makes it a crucial component in gas sensors and in the upcoming hydrogen economy [57]. Due to this, palladium-based nanomaterials have gained significant recognition in hydrogen-sensing applications, but in other sensing applications a relatively small number of reports are available, and they still have to be explored thoroughly to be recognized as credible materials for sensors [58]. Recently, a number of publications on the sensing applications of palladium-based nanostructures have appeared, but there is still a long way to go towards the realistic and broad application of palladium nanostructures in sensors for a wide range of analytes [59–61].

Due to their face-centered cubic (fcc) crystal structure, Pd NPs can be effectively prepared in a variety of morphologies such as cubes, spheres, rods, flowers, octahedrons, and so on [62]. For instance, Pd-based cubes, octahedrons, and cuboctahedrons have been fabricated exploiting the ratio of growth rates along the (111) and (100) directions [63]. Apart from shape, Pd can be easily prepared in different sizes using a variety of synthetic approaches, which also play a crucial role in the stability of the resulting material [64]. Especially at the nanoscale level, Pd-based materials demonstrate enhanced physicochemical properties, including plasmonic properties, which have led to the development of significant interest in the scientific community for Pd with controlled size and shape [65]. In this regard, Bhardawaj et al. have reported the fabrication of Pd NPs with well-defined shape and controllable size using the polyol approach [66]. These nanoparticles exhibited a hydrogen-sensing capability at room temperature; moreover, this feature was found to be shape-dependent. The hydrogen sensor studies revealed good response characteristics, and the response parameters varied with a change in shape/facet characteristics of Pd NPs. Pd demonstrates various benefits over other commonly studied plasmonic metals including Au and Ag, which make it more suitable for sensing applications [67]. Despite considerable efforts, the development of plasmonic Pd-based nanocomposites with relatively narrow optical responses while maintaining tunability, and in-depth analysis of these plasmonic materials in sensing applications, has been relatively less studied [68]. Surprisingly, Pd-based nanomaterials have demonstrated excellent plasmonic properties in terms of refractive index sensitivity or absorption capacity, which are often superior to Au or Ag nanostructures [69]. Besides this, Pd is considered as the third plasmonic material that exhibits higher stability at elevated temperatures in comparison with Au and Ag [67]. Especially for anisotropic Pd NPs, the LSPR (localized surface plasmon resonance) excitation condition for the larger axis is typically located at longer wavelengths than for Ag and Au NPs of the same size and geometry [70]. This was demonstrated by Langhammer et al. in their study: upon investigation of highly anisotropic Pd and Ag nanodisks (20 nm and 530 nm in height and diameter, respectively), it was revealed that the LSPR of Ag nanodisks appeared at a lower wavelength (1600 nm) while the LSPR of Pd nanodisks appeared at a higher wavelength (~1800 nm) [71]. Similarly, ultrathin Pd nanoplates with ~10 atomic layers and edge length of between 20 and 160 nm have demonstrated well-defined and controllable LSPRs from 826 nm to 1068 nm in the IR region [72]. These extraordinary LSPR properties of Pd NPs are highly effective in a variety of sensing applications, as various sensors are often based on changes in LSPR, which can be effectively controlled by modifications of Pd NPs' size and/or shape, which can be typically achieved during analytical assay [73]. For example, in the presence of target analytes, particle etching is either inhibited or promoted; in addition, analytes also mediate/promote the growth of particles which can facilitate control of the size, shape, and composition of particles.

Therefore, Pd NPs that have been found to possess excellent recognition in colorimetric sensors were due to the high LSPR sensitivity (large shift range) resulting from shape and size modifications [74].

Among various analytes, Pd is typically known for its high affinity towards hydrogen ( $H_2$ ); indeed, it was the first metal that was used to reversibly introduce  $H_2$  and can absorb 900 times its equivalent volume of  $H_2$ . The electronic structure of metallic Pd NPs dictates the amount of  $H_2$  absorption; indeed, the number of unoccupied d-states is directly related to the amount of absorbed  $H_2$ . The electrons from absorbed  $H_2$  are transferred to the unoccupied d-states of Pd NPs, which are transferred to Pd, and the absorption of  $H_2$  is inhibited when the unoccupied d-states of Pd are filled with electrons upon the formation of Pd hydride [75]. To overcome these and other issues, and to further enhance the sensing properties of Pd, it is typically combined with various materials including other metallic nanoparticles, metal oxide NPs, carbon-based materials, and other layered materials to fabricate different types of sensors, including electrical sensors, optical sensors, and so on.

## 2.2. Bimetallic Pd Nanocomposite-Based Sensors

Pd is typically combined with various transition metals to enhance the sensing ability of the resulting materials. In case of gas sensing including  $H_2$ , transition metals like Pt, Au, Ag, and others help to balance the number of unoccupied d-states in Pd; these metals also offer electrons to Pd, which leads to a reduction in the amount of gas absorbed [76]. The combination of Pd with other transition metals significantly reduces the cost of sensing equipment and also increases gas permeability and solubility, which ultimately leads to the inhibition of phase transition and enhanced sensing ability than pristine Pd [77]. Besides this, the alloying of Pd with other metals enhances the resistance of the gas sensor against poisoning, which leads to the generation of a stable sensor response and enhanced lifetime of the sensor [78]. Cui et al. reported the fabrication of Pd-Ag ultrathin optical film, which was used as a  $H_2$  gas sensor. In comparison with pristine Pd, the Pd-Ag hybrid has enhanced the life and the stability of sensing film [79]. In another study, Maboudian reported a modified epoxy-silver and Pd-based non-enzymatic glucose sensor. Palladium was galvanically displaced on the surface of the epoxy-silver surface in order to obtain metal nanoparticles that act as catalysts for the direct oxidation of glucose [80]. The as-fabricated sensor has shown a linear range of 1–20 mM for the detection of glucose with low interference of ascorbic acid and uric acid. A fiber-optic  $H_2$  sensor based on a hybrid of Pd and Au was reported, which consisted of a stack of Pd and Au nano-layers [81]. In this sensor, in the presence of  $H_2$ , the Pd refractive index was decreased, leading to attenuation changes in the optical fiber evanescent wave. Using this sensor, when a mixture of  $H_2$  and  $N_2$  (carrier gas) was used to test the effectiveness of the device, a response time of 4.5 s for  $H_2$  concentration of 4% was detected. Giessen et al. studied the influence of stacking order and geometry of stacked Au and Pd nanodisks on the  $H_2$ -sensing ability of a hybrid plasmonic nanostructure-based sensor [82]. Furthermore, a Pd-Au nanorod as a nanozyme was reported for malathion detection [83]. The Pd-Au nanozyme demonstrated superior peroxidase mimetic activity with O-phenylenediamine in the presence of  $H_2O_2$ . The principle of the developed assay was selective quenching of the peroxidase activity of the nanozyme, which was affected by the increasing concentration of malathion (cf. Figure 1).

Besides this, a blend of Pd and Pt was also used, such as a Pt-modified Pd-nanowire-based hybrid used as a resistive gas sensor for the detection of  $H_2$  gas in air, which was prepared with controlled Pt coverage [84]. When compared to pristine Pd nanowire, the inclusion of Pt on the surface of Pd NP changed the  $H_2$  detection properties of the resulting hybrid, including alteration of the amplitude of the relative resistance at low temperatures and fastening of the recovery rates and response at all temperatures. The heterostructured Pd-Pt core-shell nanocubes displayed catalytic activity in the glucose oxidation reaction (GOR), which was exploited in the application of non-enzymatic glucose sensors in 0.1 M  $NaOH_{(aq)}$  solution [85]. The Pd@Pt core-shell hybrid exhibited a sensitivity of  $170 \mu A \cdot mM^{-1} \cdot cm^{-2}$  under GOR catalysis conditions, and required a potential as low

as  $-0.05$  V (vs. Ag/AgCl). More recently, the surface plasmon resonance property of Pd was exploited for the quantitative SPR sensing of organic films, and for this purpose, thin films of Pd and Pt were used [86]. Moreover, a Pd and Ni alloy was also deployed, as described by Yu et al. in their study on the influence of working temperature on the accuracy of a PdNi alloy thin-film  $H_2$  sensor [87]. The PdNi  $H_2$  sensor exhibited good response to  $H_2$  with concentrations of 0.02% to 40% at room temperature, with a nonlinearly related response to  $H_2$  concentration and working temperature. The nanoporous PdNi alloy exhibited high electrocatalytic activity towards the oxidation of  $H_2O_2$  and glucose when compared to pristine Pd and Pd/C catalysts [88]. In this case, the alloy was prepared by one-step mild dealloying of PdNiAl precursor alloy in NaOH solution. The hybrid consisted of a nanoporous network architecture with a ligament size as small as 5 nm. Wang et al. developed a quick-response and revival  $H_2$  gas sensor employing Pd/Cu nanowires, which was based on a surface acoustic wave (SAW) [89]. In this case, the adsorption in Pd/Cu NWs towards  $H_2$  molecules was due to resistivity changes in the Pd NPs, which modulated the SAW propagation by an induced acoustoelectric coupling effect and sensor signal, indicating that the gas concentration was proportional to the corresponding shifts in oscillation frequency.

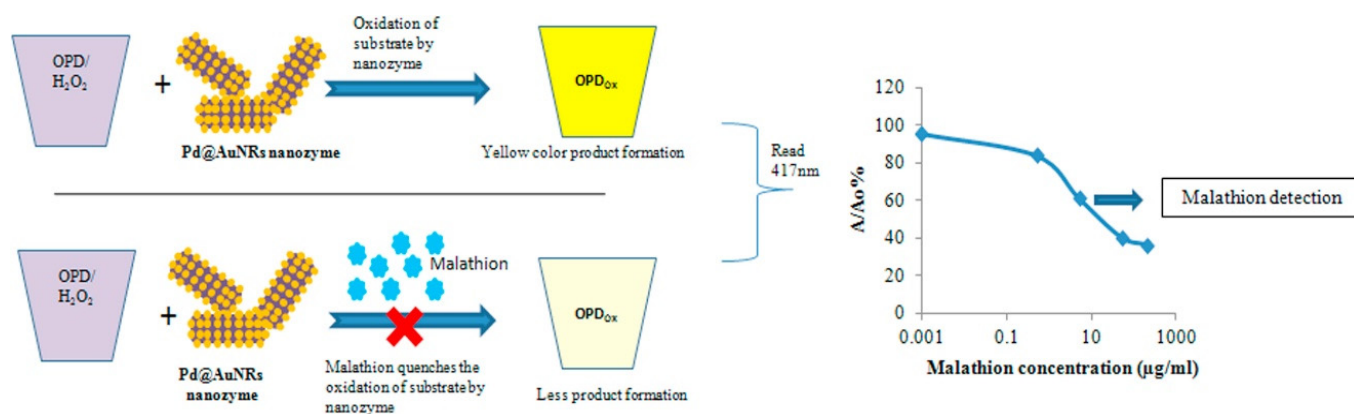


**Figure 1.** Schematic illustration of the principle of Pd@AuNR nanozyme assay for malathion [83]. Red Cross: the quenching oxidation process.

In addition to this, supported Pd bimetallic hybrids have also commonly been applied to avoid the aggregation of metallic components. For example, in a recent study, Pd and Cu hybrid nanostructures were deposited on activated carbon (AC) to fabricate a nanocomposite for electrochemical sensing of riboflavin (vitamin B<sub>2</sub>). A screen-printed electrode modified with the composite efficiently detected vitamin B<sub>2</sub>, which displayed a clear oxidation peak at  $-0.15$  V (vs. Ag/AgCl) in solutions with a pH value of 7.0. In another study, Zou et al. deposited Pd@Au core-shell (Pd@Au) heterostructures on the surface of highly reduced graphene oxide (HRG) to obtain a hybrid [90]. The hybrid was used to modify glassy carbon electrode (GCE), which was used to simultaneously determine concentrations of ascorbic acid (AA), dopamine (DA), and uric acid (UA). Similarly, in another study, Pd and Ag (70–30%) were deposited on activated ZnO thin films, which were used as a highly selective methane sensor at low operating temperature ( $\sim 100$  °C) [91]. ZnO films deposited with a Pd-Ag dotted pattern have shown high selectivity towards methane (with respect to  $H_2S$  and CO) and sensitivity ( $\sim 80\%$ ) at a comparatively low operating temperature of about 100 °C.

### 2.3. Metal Oxide-Pd NP Nanocomposite-Based Sensors

Metal oxides have gained significant recognition in sensing applications due to their excellent physicochemical properties; higher sensing response, particularly to gases; easy availability; high stability; and low cost [92]. Metal oxides are also applied in their pure forms for various sensing applications; however, most of the commonly applied metal

oxides, particularly for gas sensing, like SnO<sub>2</sub>, ZnO, In<sub>2</sub>O<sub>3</sub>, and so on, typically interact with surrounding gases at RT [93]. This seriously slows down the reaction rate and adversely affects their sensing abilities [94]. Thus, specialized catalysts are required to lower the activation energy of the reaction, which ultimately accelerates the chemical reactions for fast and high responses [95]. To resolve these issues in gas sensors, particularly in H<sub>2</sub> sensors, noble metals like Pd and Pt are applied due to their high catalytic properties for H<sub>2</sub> dissociation [96]. The dissociated H<sub>2</sub> atoms typically move from the Pt or Pd parent particles to the neighboring metal oxides and initiate chemical reactions, which has been known as the “spillover effect” [97]. Thus, Pd has been incorporated with a variety of metal oxides; for example, Tong et al. introduced an easy method for the decoration of WO<sub>3</sub> nanorods with Pd NPs to obtain enhanced NH<sub>3</sub> gas-sensing performance [98]. In addition, Liu et al. reported the shape-controlled preparation of Pd nanocubes on WO<sub>3</sub> nanoplates using a solvothermal approach; the resulting hybrid demonstrated a high and fast response at room temperature for H<sub>2</sub> sensing [99]. They also investigated the relationship between the interaction of Pd nanocrystals with metal oxides and their effect on sensing performance by comparing the sensing performance of pure WO<sub>3</sub> and mechanically mixed Pd nanocubes and WO<sub>3</sub> nanoplates. In freestanding Pd nanocrystals, H<sub>2</sub> dissociation occurs on Pd while reactions resulting in resistance changes take place on metal oxides. More recently, Lee et al. reported a chemiresistive sensor based on Pd-WO<sub>3</sub> to detect H<sub>2</sub> at the ppm level at RT with a outstandingly high response along with extraordinary selectivity [100]. The composite was prepared by using a self-assembly approach, in which the self-assembly of Pd NPs and WO<sub>3</sub> nanoparticles was reinforced with positively charged droplets.

Apart from WO<sub>2</sub>, SnO<sub>2</sub> is also the most used metal oxide, particularly in gas sensing, due to its stability: for example, SnO<sub>2</sub> NP-based sensors for the detection of volatile organic compounds (VOCs), carbon monoxide (CO), etc., at low temperature. In particular, in the case of CO, SnO<sub>2</sub> responded to CO via oxidation of CO molecules by chemisorbed oxygen species to CO<sub>2</sub> [101]. Subsequently, considerable changes in charge carrier density occurred on the surface, leading to changes in resistivity. However, low-temperature sensing of CO faces long-term stability problems and often requires high power consumption. To overcome these issues, the incorporation of additive metals including Pd is crucial to improve sensitivity and selectivity, resulting in sensors which also lower the operating temperature. For instance, Kim et al. demonstrated the fabrication of a low-temperature sensor for CO detection using Pd/SnO<sub>2</sub> nanocomposite, which is prepared by an infiltration process [102]. The addition of an organic binder (15% hydroxypropyl cellulose (HPC)) led to several improvements in sensor efficiency, including high sensitivity to CO gas at the ppm level, efficient repeatability in 6–18 ppm CO exposure, and active response for more than 40 days. Similarly, a CO sensor based on nanocrystalline Pd/SnO<sub>2</sub> was reported by Gangwar et al.; thin films of the as-prepared hybrid were deposited on an alumina substrate by reactive magnetron sputtering for highly sensitive and selective CO gas sensing [103]. In another case, an ultra-fast-response H<sub>2</sub> sensor based on Pd-modified SnO<sub>2</sub> NPs with a size of ~7 nm was evaluated. The addition of Pd significantly enhanced the H<sub>2</sub> sensing performance when compared to a pristine SnO<sub>2</sub> gas sensor; in particular, after Pd addition, the working temperature of SnO<sub>2</sub> decreased from 300 °C to 125 °C [104]. Several studies have suggested that the incorporation of noble metal decoration including Pd enhances the sensing properties of the resulting hybrids due to the electronic sensitization as well as chemical sensitization effects of metals [105]. In the case of chemical sensitization, metals catalytically influence the dissociation of oxygen and some target gases, leading to easier and faster adsorption on the surface of the gas sensor [106]. However, electronic sensitization causes the creation of a junction potential barrier between the sensing material and the metallic NPs [107]. Differences in the Fermi levels of the sensing material and the metallic NPs often cause the depletion/accumulation of charge carriers at the metal oxide near the metallic NPs, eventually leading to enhancement in the sensor signal. Therefore, application of a sensing layer composed of metal oxide, noble metal, and oxygen vacancies has been proposed by several researchers to enhance gas-sensing properties. In this regard,

Choi et al. used highly catalytic Pd-implanted  $\text{SnO}_{2-x}$ -decorated  $\text{SnO}_2$  nanowires for  $\text{NO}_2$  gas sensing. In this case, Pd NPs were surrounded in  $\text{SnO}_{2-x}$  with a large number of structural defects on the surface of  $\text{SnO}_2$  nanowires for enhancing  $\text{NO}_2$  sensing [108]. They also studied in detail the underlying sensing mechanism in terms of generation of oxygen defects, catalytic activity of Pd, and creation of heterojunctions in the sensing material (cf. Figure 2).

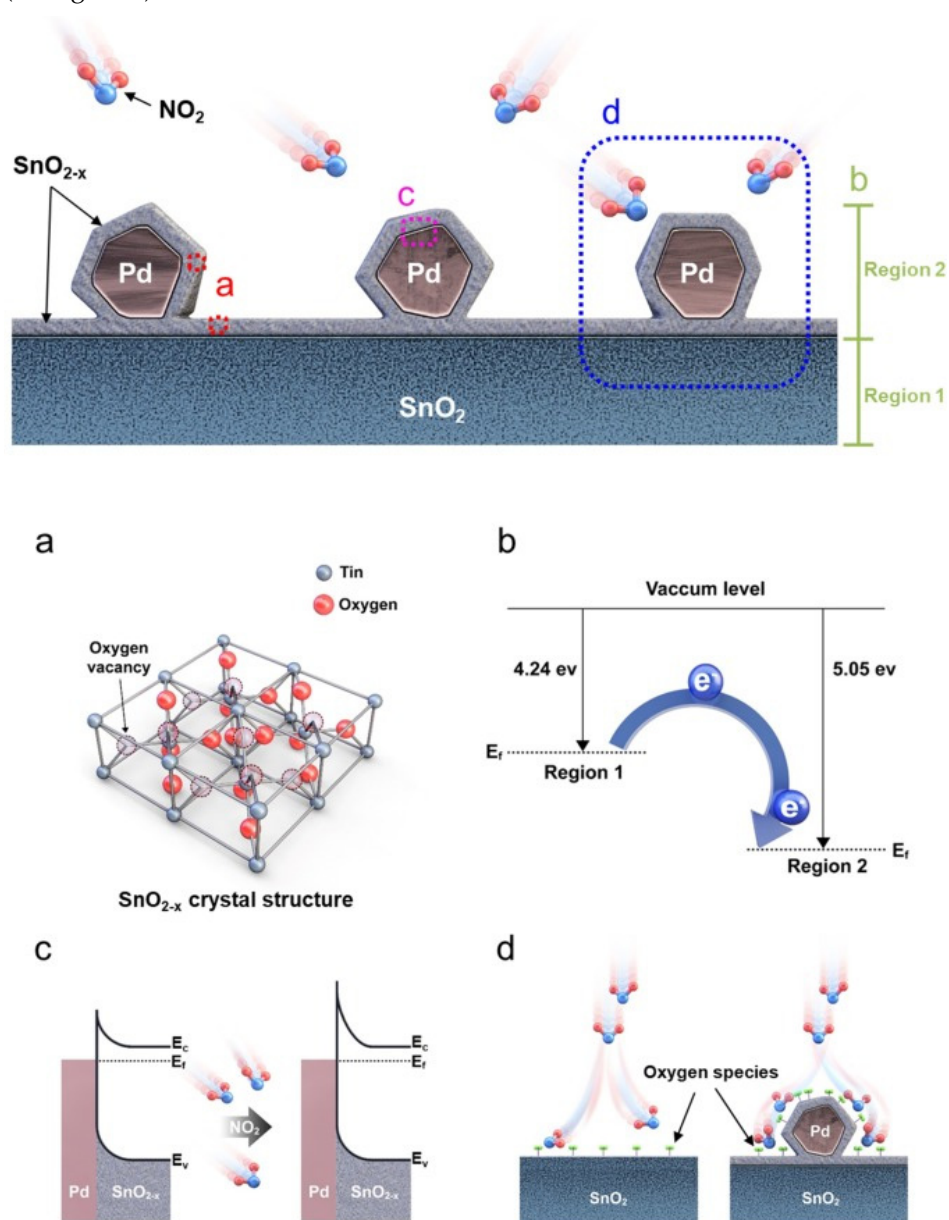


**Figure 2.** Schematic diagrams explaining sensing mechanisms on the surface of gas sensors (a) Crystal structure of  $\text{SnO}_{2-x}$  with oxygen vacancy, (b) Comparison of the Fermi levels and work functions of the two samples; electrons will transfer from the core toward the shell, (c) Interface between Pd and  $\text{SnO}_{2-x}$  and (d) Spillover effect of catalyst [108].

In addition, ZnO, which is an n-type semiconductor with a band gap of 3.37 eV, and Pd as a noble metal, were also desirable choices for the fabrication of a variety of sensors including a planar-type gas sensor [109]. For instance, Wang et al. fabricated a Pd-modified ZnO nanocomposite using a simple hydrothermal route and subsequent calcination process [110]. The as-prepared composite was tested for its methane ( $\text{CH}_4$ )-sensing properties, which were also compared with those of pure ZnO, and the materials exhibited a noticeable sensing capability even at the smallest loading of Pd. The 1% Pd-

ZnO exhibited a maximum response value of 19.20 to 5000 ppm CH<sub>4</sub> at 200 °C, but also exhibited excellent selectivity and good repeatability. In another study, thin-film ZnO chemoresistive acetone sensors were fabricated by the decoration of Pd NPs on the surface at low operating temperatures [111]. The polycrystalline ZnO films were crystallized at the (002) and (101) orientations of the hexagonal phase; due to this, the ZnO:Pd sensor showed a lower detection limit and a response enhancement factor of between 2 and 7 compared with pure ZnO sensors. Recently, Pd-decorated ZnO NPs were supported on a highly porous framework of activated carbon to achieve an efficient electrochemical sensor for the detection of carbaryl trace [112]. The results revealed a unique oxidative-sensing ability of composite for carbaryl at 0.62 V with a low  $\Delta E$  (80 mV) as compared to that of a bare glassy carbon electrode (GCE). Under optimized conditions, electrochemical sensing of carbaryl was realized with a low detection limit of 0.01  $\mu\text{M}$  and a detection range of 0.01–5.0  $\mu\text{M}$ . Apart from these oxides, a variety of other metal oxides have also been chosen to fabricate sensors for the detection of a range of analytes [113]. Pd-In<sub>2</sub>O<sub>3</sub> nanocomposites were prepared by Pd modification, and the composite was applied for room-temperature H<sub>2</sub> sensing [114].

#### 2.4. Carbon Materials and Pd Nanocomposite-Based Sensors

Carbon-based nanomaterials such as single and multiwalled carbon nanotubes (SWCNTs, MWCNTs), graphene, carbon nitrides, fullerenes, and several others have been considerably popular as sensor materials due to their remarkable properties [115,116]. An example of this is their ability to hybridize into sp, sp<sup>2</sup>, and sp<sup>3</sup> configurations based on the bonding relationships with neighboring atoms, and the narrow gap between the 2s and 2p electron shells, effectively facilitating the fabrication of a wide variety of carbon materials [117,118]. In particular, as electrode materials in sensors, carbonaceous nanomaterials demonstrate several unique properties for sensing and detection of a variety of analytes [119], such as the possibility of depositing electrocatalytic groups on the surface of these materials, the presence of edge-plane-like sites located at the ends and in defect areas of nanostructures, high surface area, efficient electronic properties, and unique 2D structures, such as in graphene and carbon nitride, etc. [120]. In addition to this, carbon nanostructures are also beneficial due to their low weight and low cost, and also exhibit onboard reversibility and rapid sorption kinetics [121]. Besides this, carbon nanostructures offer high stability in basic and/or acidic media, are relatively inexpensive, are easily recoverable, and are considered the best support material [122]. As effective support materials, they are extremely capable of enhancing the electroactive area with excellent nanoparticle dispersion and the promotion of electronic transfer and improvement of the rate of diffusion of electroactive species through the porous structure of the carbon support [122]. Due to these excellent properties, a variety of carbon nanostructures have been effectively combined with Pd NPs to fabricate highly advanced and efficient sensors [123]. For example, porous activated carbons (PACs) derived from biomass feedstock have gained significant recognition in sensing and detection of toxic metal ions and other analytes [124]. Pd NP-decorated PAC-modified GCEs have been successfully utilized as potential electrochemical sensors for the detection of gases including H<sub>2</sub> and methane and biomolecules such as uric acid, glucose, dopamine, ascorbic acid, and hydrazine [125–127]. For instance, Veerakumar et al. prepared PACs derived from waste biomass feedstock (fruit peels). The as-prepared PACs were decorated with Pd and used to modified GCEs [128]. The PAC-Pd-modified electrodes were used as electrochemical sensors for the detection of different types of toxic heavy-metal ions, including Cd<sup>2+</sup>, Pb<sup>2+</sup>, Cu<sup>2+</sup>, and Hg<sup>2+</sup>, which showed superior performances for both individual as well as simultaneous detections. Similarly, Zhang et al. fabricated a uniformly decorated Pd NP- and PAC-based composite, in which the Pd NPs were in situ reduced on PAC (Pd@PAC) via KOH activation and a thermal reduction method [129]. The Pd@PAC-modified GCE was applied for the detection of trace Cd<sup>2+</sup>, Pb<sup>2+</sup>, and Cu<sup>2+</sup> ions by square-wave anodic voltammetry (SWASV). The as-fabricated sensor has demonstrated extreme sensitivity and selectivity during the detection of heavy-metal ions.

Among carbon materials, graphene is more popular due to its planar sheetlike structure consisting of  $sp^2$  hybridized carbon atoms [130]. In this unique structure, the strongest bond is the in-plane  $\sigma_{C-C}$  bond, and the out-of-plane  $\pi$  bond is responsible for the electron conduction of graphene, which offers weak interaction among graphene layers or between graphene and the substrate [131]. Due to this unique electronic configuration, graphene consists of a large surface area ( $2630 \text{ m}^2 \text{ g}^{-1}$ ); high mechanical strength (200 times greater than steel); high electrical conductivity, which is 60-fold greater than single-walled CNT (SWCNT) and 6-fold higher than that of copper; along with high elasticity and thermal conductivity [132]. Thus, graphene-based electrodes exhibit excellent electronic conductivities and high electrocatalytic properties when compared to other carbonaceous nanostructures [133]. In particular, studies have revealed that the combination of graphene with noble metal nanoparticles has potentially enhanced the electrocatalytic performance of the resulting nanocomposites [134]. Graphene- and Pd NP-based nanocomposites have especially been extensively explored for the determination of various analytes because of their excellent electrocatalytic properties [135]. These composites have been prepared by various approaches including in situ electrodeposition from a Pd precursor solution or immobilization of pre-synthesized Pd nanoparticles onto electrodes [136]. The composite was used to fabricate a selectivity-enhanced field-effect transistor (FET)-type glucose sensor, employing surface functionalization phenomena using electrodeposition and spin coating techniques [137]. In another study, a novel and sensitive electrochemical nitrite sensor was fabricated using in situ electroless deposition of Pd NPs and rGO in a stepwise manner on a GCE. The Pd-rGO-modified electrode demonstrated considerable enhancement towards the oxidation of nitrite with increased current response and reduced overpotential, which was a result of the synergistic catalytic effect of rGO and Pd NPs. Recently, there has been the highly selective detection of chloramphenicol (CAP) using a Pd NP-decorated highly reduced graphene oxide (rGO-PdNP) nanocomposite [138]. The rGO-PdNP-modified GCE exhibited excellent electroactivity in the presence of chloramphenicol, which demonstrated an outstanding performance with a linear response range of 50–1000 nM and a low detection limit of 50 nM ( $S/N = 3$ ). In another study, Pd NPs were successfully decorated on polypyrrole/reduced graphene oxide substrate to obtain rGO/Pd@PPy nanocomposite [139]. Using this, an effective electrochemical sensor was fabricated by depositing the as-prepared composite on GCE for the simultaneous detection of ascorbic acid (AA), dopamine (DA), and uric acid (UA) (cf. Figure 3). The modified electrode showed excellent catalytic efficiency and conductivity for the detection of the aforementioned analytes with higher current and oxidation peak intensities, while the simultaneous detection of these molecules was achieved due to the elevated selectivity and sensitivity of rGO/Pd@PPy NPs.

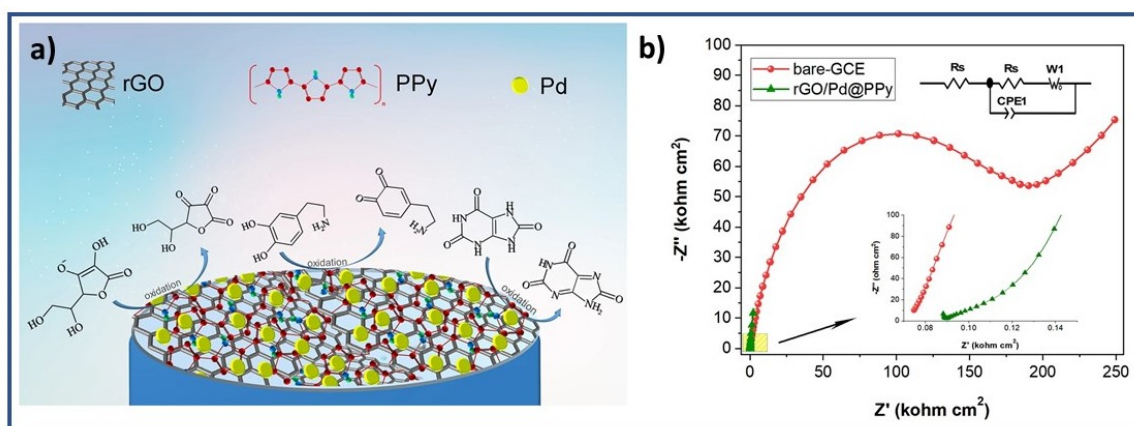


**Figure 3.** (a) A schematic diagram for the electrochemical oxidation process of AA, DA, and UA at the surface of rGO/Pd@PPy biosensor. (b) Nyquist plots of bare-GCE and rGO/Pd@PPy-modified electrodes [139].

Apart from this, carbon nitride is another metal-free carbon material, which exhibits a high N : C ratio with structure ranging from a polymeric to a graphitic form, constituting heptazine or triazine rings as structural motifs [140]. These materials consist of medium band gap, porosity, and high thermal and chemical inertness; in addition, due to the tunability of their electronic and optical properties, biocompatibility, high stability, and low cost, they can be employed in the field of sensing [141]. In a study, carbon nitride was combined with Pd to fabricate a room-temperature H<sub>2</sub> sensor [142]. Graphitic carbon nitride (g-C<sub>3</sub>N<sub>4</sub>) was prepared by pyrolysis of melamine. Pd NPs were scattered on g-C<sub>3</sub>N<sub>4</sub> by the polyol reduction method. Hydrogen-sensing properties of Pd/g-C<sub>3</sub>N<sub>4</sub> were studied within a near-flammability range of 1–4 vol%. More recently, the deposition of Pd/g-C<sub>3</sub>N<sub>4</sub>-based thin films at different percentages of Pd loading (10%, 20%, and 40%) on an Astro-glass substrate in a temperature range of 350–400 °C was reported. These films were applied for efficient H<sub>2</sub> gas sensing at RT. Among various films, 40% Pd/g-C<sub>3</sub>N<sub>4</sub> and 20% Pd/g-C<sub>3</sub>N<sub>4</sub> showed response and recovery, while the sensitivity of 20% Pd/g-C<sub>3</sub>N<sub>4</sub> was found to be highest amongst all differently loaded composites.

### 2.5. Multicomponent Pd Nanocomposite-Based Sensors

To overcome the issues faced by bimetallic hybrids, such as their metastable nature and lower kinetics, Pd-based multicomponent hybrids like ternary nanocomposites, etc., have been applied, which exhibit higher kinetics even at low temperatures. Multicomponent hybrids have been shown to have higher permeability than pure Pd, as reported by Tarditi et al. [143]. In their study, it was revealed that the H<sub>2</sub> permeability of ternary Pd composite (PdAgCu) demonstrated four times higher H<sub>2</sub> permeability than its binary counterpart with an *fcc* phase. Furthermore, to reduce the detection limit of analytes and to enhance response and selectivity, controlling the microscopic morphology of multicomponent composites is necessary through the targeted selection of catalytic elements. In this regard, the ternary porous H<sub>2</sub> sensors of Pd-doped spherical SnO<sub>2</sub> loaded on highly reduced graphene oxide (HRG) was synthesized by a simple, template-free hydrothermal method. The influence of different HRG mass ratios and Pd molar ratios on the H<sub>2</sub>-sensing properties of SnO<sub>2</sub>-based materials was systematically analyzed. Due to its synergistic effect, the 5.0 Pd-SnO<sub>2</sub>/HRG ternary nanocomposite showed the best H<sub>2</sub>-sensing properties, and displayed a response of 32.38 to 200 ppm hydrogen at 360 °C. Based on its surface oxygen vacancies and its reaction kinematics, the mechanisms of high sensitivity and selectivity of the 5.0 Pd-SnO<sub>2</sub>/rGO material to a low concentration of H<sub>2</sub> were described.

In another study, to compare the sensing properties of binary and ternary composites of Pd for sensing applications, binary WO<sub>3</sub>-graphene and ternary WO<sub>3</sub>-graphene-Pd hybrids with varied contents of graphene and Pd were prepared by a microwave-assisted hydrothermal method [144]. Due to the superior catalytic property of Pd, H<sub>2</sub> molecules were effectively disintegrated into H<sub>2</sub> atoms, which enhanced the activity and improved the gas-sensing abilities of the resulting material. On the other hand, due to high electrical conductivity, graphene served to augment the mobility of charge carriers within the ternary materials, which accelerated the response/recovery rates of gas sensors. The graphene and Pd, with separate work functions from WO<sub>3</sub>, facilitated the creation of a heterojunction at the interface of these diverse materials, which led to the enhancement of the property of electron-hole pair separation and further amplified the gas-sensing performance of the ternary materials. In case of multicomponent nanocomposites, the sensing performance is commonly dependent on the uniformly distributed heterojunctions. To study this, different ratios of CoTiO<sub>3</sub> (CT) and TiO<sub>2</sub> (T) were explored at RT of 25 °C for sensing benzene. The gas-sensing performance of the sensor was further improved by the construction of a Pd-CTT ternary composite sensing material [145]. The excellent sensing property of the Pd-CTT sensor towards benzene is associated with the formation of a CoTiO<sub>3</sub>/TiO<sub>2</sub> p-n heterojunction and the catalytic action of Pd. The Pd-CTT sensor showed a high response ( $R_g/R_a = 33.46 @ 50 \text{ ppm}$ ) to benzene, with a detection limit as low as 100 ppb. In another study, halloysite nanotube@Pd-molybdenum disulfide (HNTs@Pd-MoS<sub>2</sub>) ternary

composite (HNTs@Pd-MoS<sub>2</sub>) was fabricated, which was applied for the electrochemical determination of dopamine [146]. The as-fabricated sensor exhibited significant response for the electrocatalytic oxidation of dopamine with typical linearity in the concentration range of 25–1000  $\mu\text{M}$ , with a LOD of 0.15  $\mu\text{M}$ . Besides this, the ternary composite HNTs@Pd-MoS<sub>2</sub> was also effective for the detection of uric acid, glucose, ascorbic acid, and acetaminophen. Recently, Pd NP-functionalized, rGO (highly reduced graphene oxide) nanosheet-modified 3D rod-like CuO (Pd-CuO/rGO) with a nanowire hierarchical structure was fabricated, which was highly effective for the trace-level detection of NO<sub>2</sub> gas at RT [147]. The Pd-CuO/rGO hybrid showed an ultra-high response of 64.2 to 100 ppm NO<sub>2</sub> gas at RT, which is  $\sim 3.4$  times that of the pristine CuO sensor, 2.7 times that of the Pd-CuO sensor, and 2 times that of the CuO/rGO sensor, respectively. Simultaneously, a response/recovery time of 10.7/9.2 s to 10 ppm NO<sub>2</sub> gas at RT was indicated for the Pd-CuO/rGO sensor.

Zou et al. fabricated Pd@Au core-shell (Pd@Au) heterostructures using Pd nanocubes as the structure-directing cores [90]. The as-prepared Pd-Au core-shell (Pd@Au)/RGO hybrid was applied to modify GCE and utilized for the simultaneous determination of the concentrations of ascorbic acid (AA), uric acid (UA), and dopamine (DA). In a more detailed analysis, Ghosal et al. comparatively explored the sensing abilities of diverse metal-oxide-based ternary hybrids such as Pd/RGO/TiO<sub>2</sub> nanotubes (NTs), Pd/RGO/WO<sub>3</sub> nanoflowers (NFs), and Pd/RGO/MnO<sub>2</sub> nanoflowers (NFs) [148]. Every ternary hybrid metal oxide was a crucial sensing matrix because of their high surface-to-volume ratio and large number of adsorption sites, which enhanced the sensitivity or response magnitude (%RM) of the sensor. On the other hand, RGO exploited the high mobility ( $\sim 1600 \text{ cm}^2/\text{V}\text{-s}$ ) and acted as a connector for the materials involved, which led to the enhanced response or recovery kinetics. Finally, Pd NPs helped to reduce the activation energy requirement for targeted species dissociation, due to their catalytic activity, which significantly reduced the operating temperature. These ternary hybrids were applied for the detection of a variety of volatile organic compounds (VOCs), such as methanol, ethanol, etc. Among these, all the hybrids were most effective in the detection of alcohol with a detection range of 1–700 ppm and a fast response time ( $\sim 12\text{--}20$  s) and recovery time ( $\sim 23\text{--}30$  s) without conceding the response magnitude (80–98% at 700 ppm). More recently, an efficient methane sensor was fabricated which was based on core-shell-structured ZnO/Pd@ZIF-8. The Pd-based hybrid was fabricated via the self-templated method, and the resulting hybrid sensor displayed excellent selectivity towards CH<sub>4</sub> against NH<sub>3</sub>, CO, and NO<sub>2</sub> [149].

Other studies involving ternary composites consisting of multi-metallic and multi-metal-oxide nanostructures together with Pd have also been reported [150]. For example, in a recent study, a ternary catalyst consisting of a Pd-Cu-Ni nanocomposite which was electrodeposited at rGO-modified GCE (Pd-Cu-Ni/rGO/GC) is reported [151]. The modified electrode gas demonstrated excellent activity towards glucose electrooxidation reaction (GOR); at the surface, the peak current was 4.6, 3.0, and 2.2 times higher than that of individual hybrids with single metals such as Cu/rGO/GC, Pd/rGO/GC, and Ni/rGO/GC electrodes, respectively. In this case, graphene augmented the surface area, durability, and electrical properties of the catalyst, whereas Pd offered plenty of active sites during GOR activities. Zhang et al. prepared PdNPs@ZnO-Co<sub>3</sub>O<sub>4</sub> using oxidation treatment of a bimetallic ZnCo-zeolitic-imidazolate framework (ZnCo-ZIF); the Pd precursor was subsequently reduced in situ by a chemical process on the surface of the nanocrystal. The as-obtained hybrid was later combined with MWCNTs (multiwall carbon nanotubes) to obtain PdNPs@ZnO-Co<sub>3</sub>O<sub>4</sub>-MWCNTs hybrids, which are utilized as electrodes for a non-enzyme electrochemical sensor for high-sensitivity detection of tanshinol [152]. With PdNPs@ZnO-Co<sub>3</sub>O<sub>4</sub>, and the excellent charge transfer property between imidazole groups of the ligands in MOFs and MWCNTs, the sensor showed high sensitivity for tanshinol detection under optimum experimental conditions. The sensor showed two good linear relationships between the current and tanshinol concentration in the ranges of 0.002–0.69 mM ( $R^2 = 0.989$ ) and 0.69–3.75 mM ( $R^2 = 0.994$ ) with corresponding sensitivities of 59.16  $\mu\text{A mM}^{-1}$  and 19.08  $\mu\text{A mM}^{-1}$  together with an LOD of 0.019  $\mu\text{M}$  ( $S/N = 3$ ).

### 3. Environmental Redemption Application

The recent increase in the number of pollutants produced by the industrial sector affects the life of living organisms. The main types of contaminant are heavy metals, oil spills, herbicides, fertilizers, organic compounds, organic dyes, and sewage, which have high toxicity and are hazardous to the health of humans [39]. Global organizations and researchers are making a great effort to reduce the number of contaminants in water and the environment by using different methods such as coagulation [153], chemical reduction [154], reverse osmosis [155], and photodegradation procedures [156] to remove nitro compounds and organic dyes [157] (cf. Table 1). However, the effort has been focused on using noble metal nanoparticles such as gold, palladium, silver, platinum, and copper as catalysts to eliminate pollutants from water and the environment due to these metals being eco-friendly and high-activity sites [157].

**Table 1.** Reported catalysts for environmental remedy applications.

Catalyst	Application	Catalyst Loading	Temp	Time	Yield %	Ref.
PEI-Pd	reduction of 4-NP to 4-AP	20 mg	RT	-	94	[158]
Pd-CNT-GH	reduction of 4-NP to 4-AP	5 mg	-	30 s	100	[159]
Pd NPs/Fe <sub>3</sub> O <sub>4</sub> @nanocellulose catalyst	reduce Cr(VI) to Cr(III)	0.4 g/L	50 °C	40 min	-	[160]
CuPd@ZIF-8	reduce Cr(VI) to Cr(III) in an aqueous solution	20.0 mg	-	60 min	89	[161]

Proven hydrogels are effective in adsorbing contaminants by coordination, complexation, chelation, ion exchange, adsorption by physical forces, and ion trapping in their inter- and intra-fibrillar capillaries [158]. Several hydrogels have a great number of polar functional groups, for instance, hydroxyl and carboxyl groups [162], which can robustly chelate with transition metals (Au<sup>57</sup>, Ag<sup>58</sup>, Cu<sup>59</sup>, Pd<sup>60</sup>, Ni<sup>61</sup>, Co<sup>62</sup>, etc.), causing the successful loading of metal nanoparticles and prohibiting their aggregation [163]. Recently, palladium-based hydrogels have been used as catalysts for the reduction of nitrophenols (which have high toxicity and are a reason for cancer) to aminophenols due to significant merits such as thermal stability, high mechanical strength, reusability, easy work-up, simple synthesis, and high surface area [164].

On the other hand, hexavalent chromium (Cr(VI)) is one of the largest pollutants in the environment caused by industries such as metal finishing, electroplating, leather tanning, dyeing, and textiles. Thus, Cr(VI) is highly toxic, carcinogenic, and a confirmed mutagen [165,166]. In contrast, a small concentration of Cr(III) is needed for nutrient composition, such as sugar and fat metabolism in the human body, so Cr(III) could be degraded into various neutral, polynuclear, and other hydroxide species in an aqueous medium [167]. Consequently, many researchers have been interested in reducing Cr(VI) to Cr(III) through several methods and eco-friendly strategies [14,163,166,168]. Kalantari et al. successfully prepared a Pd NPs/Fe<sub>3</sub>O<sub>4</sub>@nanocellulose catalyst to reduce Cr(VI) to Cr(III) in an aqueous medium (formic acid) (cf. Figure 4). Pd NPs/Fe<sub>3</sub>O<sub>4</sub>@nanocellulose was prepared without using any chemical reducing agent, which depended on the roots of *Chelidonium majus* aqueous extract as a reduction agent to reduce Pd (II) to Pd nanoparticles. However, the Fe<sub>3</sub>O<sub>4</sub>@nanocellulose catalyst was not highly efficient in reducing Cr(VI) to Cr(III) and also needed more time to finish the reaction, while Pd NPs/Fe<sub>3</sub>O<sub>4</sub>@nanocellulose was proven efficient in reducing Cr(VI) during a short time in formic acid due to an increase in Pd NPs activity site and the surface area. Firstly, FA is adsorbed on the Pd surface, and then it decays to provide CO<sub>2</sub> and H<sub>2</sub>; the existence of Pd NPs helps to raise the amount of adsorbed H<sub>2</sub> on the activity site, which acts as reducing agent for the reduction of Cr(VI) to Cr(III) [160].

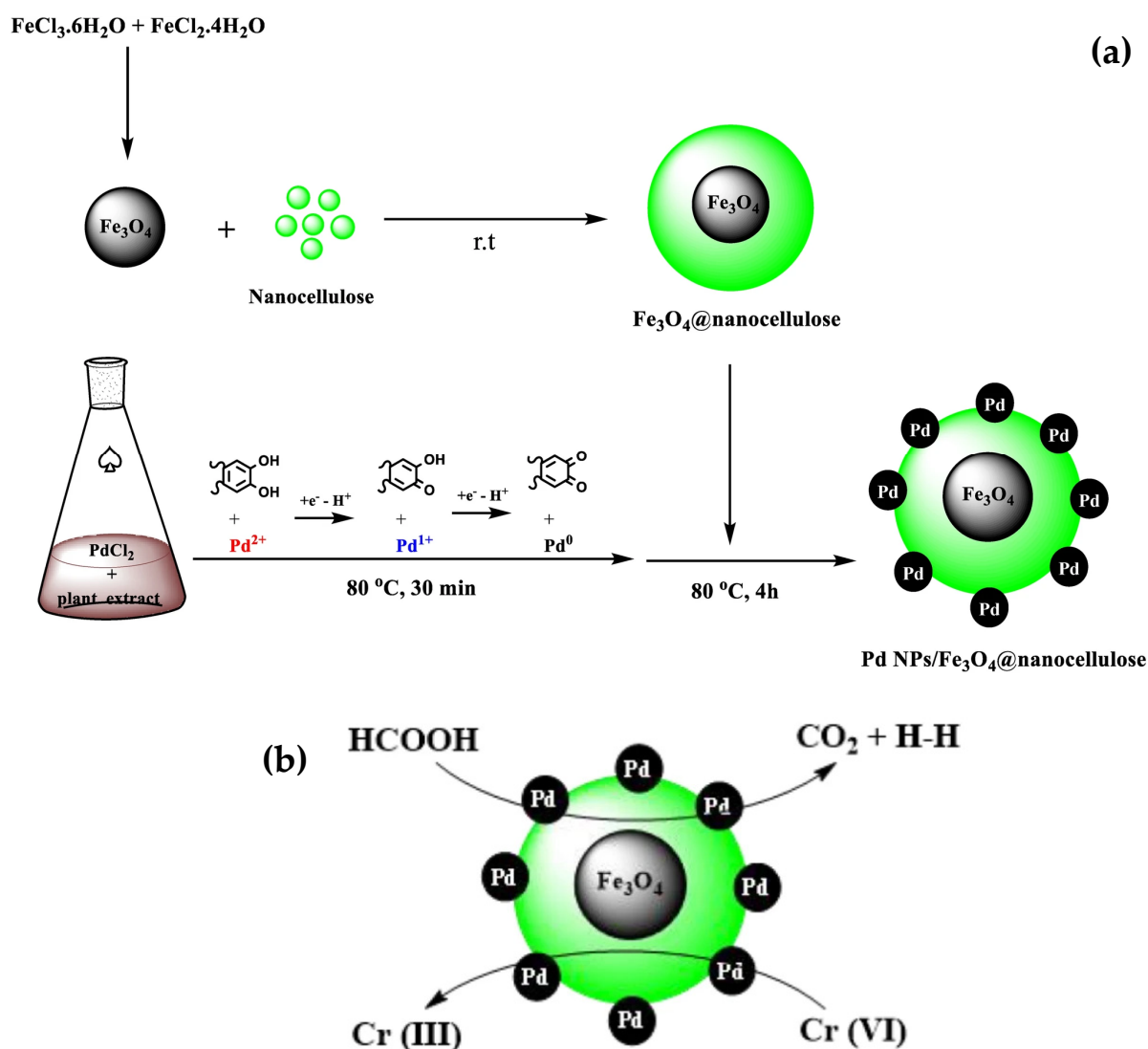


**Figure 4.** Schematic illustration for the (a) green synthesis of Pd NPs/ $\text{Fe}_3\text{O}_4$ @nanocellulose catalyst and (b) reduction of Cr(VI) to Cr(III) on Pd NPs/ $\text{Fe}_3\text{O}_4$ @nanocellulose catalyst in the presence of formic acid [160].

Much research has proven that noble-metal loading on metal-organic frameworks (MOFs) has improved photocatalytic activity [164]. Zhang and co-workers synthesized a CuPd@ZIF-8 catalyst by using a sol-gel method (cf. Figure 5). ZIF-8/CuPd NPs displayed higher efficiency than ZIF-8 due to Cu/Pd-enhanced photocatalysis. Moreover, bimetallic catalysts displayed higher catalytic activity and selectivity for target products. Among these, CuPd can work as an electron intermediary to improve conductivity, so the transfer of electrons from Cu to Pd leads to an enhanced electron density of Pd atoms, thus favoring the adsorption of the intermediate format and succeeding generation of active H atoms over ZIF-8/CuPd NPs. Thus, using the photoreduction method, ZIF-8/CuPd NPs were used to reduce Cr(VI) in an aqueous solution [161].

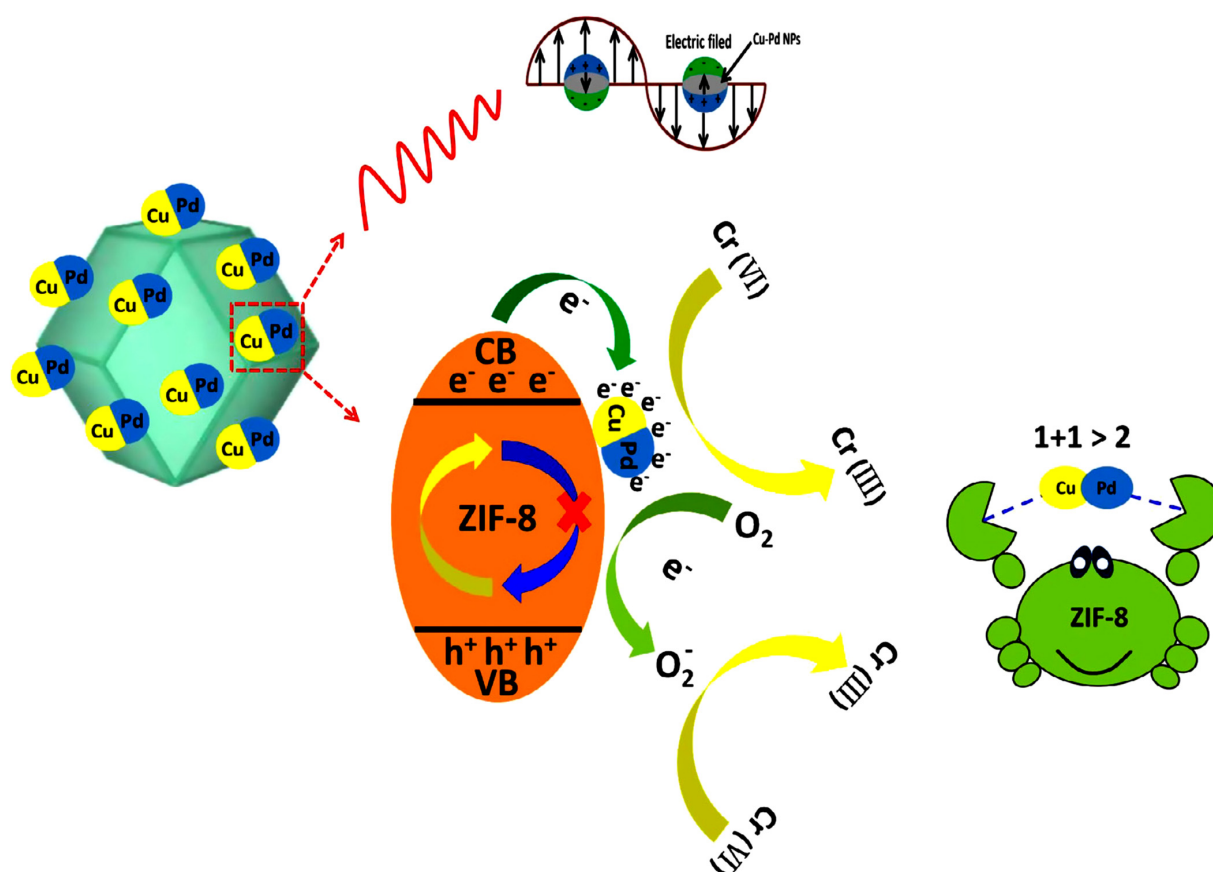


Figure 5. Schematic illustration of the Cr(VI) degradation mechanism [161].

#### 4. Pd Nanoparticles in Organic Synthesis

Pd nanoparticles are earning notable attention because of their unique competence as a catalyst in a large number of organic transformations, including several types of cross-coupling, carbon-carbon, redox, and hydrogenation reactions. They play a vital role in several industrial heterogeneous catalysts due to their unique properties: for instance, a well-defined structure; great intrinsic carrier; and outstanding electronic, thermal, and mechanical stability [169]. Moreover, palladium-based catalyst was used in organic transformations such as Heck, Stille, Suzuki-Miyaura, Hiyama, Sonogashira, and Buchwald-Hartwig coupling and asymmetric arylation, allylation, reduction, cyanation, carbonylation, and condensation reactions (cf. Table 2) [46,170]. However, due to low selectivity, activity, and high cost, the industrial chemical synthesis has observed a reduced usage of Pd-based catalysts. There are many efforts to improve Pd-based catalysts by merging multiple metals with Pd to improve the selectivity and activity of Pd-based catalysts.

Table 2. Pd nanoparticles reported in different organic syntheses.

Catalyst	Application	Catalyst Loading	Temp	Time	Yield %	Ref.
NPs@Fe <sub>3</sub> O <sub>4</sub> /CS-AG	produce 4-Iodobiphenyl	$1.5 \times 10^{-2}$ mmol	-	5 min	99	[171]
nano-Pd/chitosan	produce pyrazolyl	0.02 mol%	60 °C	60 min	99	[172]
g-C <sub>3</sub> N <sub>4</sub> /PANI/PdNPs	methanol oxidation	0.5 g	-	30 min	-	[173]
PdPGO	energy storage	-	-	-	88	[174]
Pd-BiVO <sub>4</sub>	produce H <sub>2</sub> O <sub>2</sub>	0.1 wt%	-	2h	-	[175]

#### 4.1. Pd Nanocatalyst for Cross-Coupling Reactions

Cross-coupling is a creative method to format a single bond between carbon C-C, C-H, C-S, C-N, C-O, and so on to synthesize complex organic compounds. Moreover, cross-coupling reactions are used to prepare many natural products and compounds with complex chemical structures that are physiologically active [176]. In 2010, the Noble Prize was given to Richard F. Heck, Ei-Ichi Negishi, and Akira Suzuki for the discovery of Pd-catalyzed cross-coupling reactions in organic synthesis [177]. Suzuki-Miyaura cross-coupling (SM) reactions generally include the reaction between aryl boronic acid and aromatic halides [178]. However, Pd catalysts have encountered some obstacles, such as low efficiency in separation limit, metal leaching, and insufficient selectivity. In this regard, effort has been dedicated to modify Pd-based catalysts to overcome obstacles caused by synthesis of Pd catalysts on the nanoscale and immobilizing them on a solid surface [179]. Baran and co-worker synthesized a Pd NPs@Fe<sub>3</sub>O<sub>4</sub>/CS-AG catalyst and tested its performance in Suzuki-Miyaura reactions: that is, the reaction of phenylboronic acid with 4-iodoanisole under solvent-free and microwave irradiation. A high yield was noticed when Pd NPs@Fe<sub>3</sub>O<sub>4</sub>/CS-AG catalyst was used compared with other catalysts [171]. Senthilkumar et al. prepared a nano-Pd/chitosan catalyst and used it in a Suzuki coupling reaction to synthesize pyrazolyl derivatives from reacting aryl boronic acid with a heterocyclic halide. The result was optimal and obtained a high yield due to the efficiency of the activity site and large surface area [172].

#### 4.2. Pd Nanocatalyst for Organic Redox Reactions

The unique properties of Pd NPs, such as amazing electro-oxidation properties, homogeneous dispersion, electrode stability, and quick electron transfer characteristic features, has led to a rise in the catalytic performance of hybrid combinations. Owing to these properties, it was used in fuel cell applications and electro-oxidation reactions [180].

Eswaran et al. reported producing efficient methanol electro-oxidation after using g-C<sub>3</sub>N<sub>4</sub>/PANI/PdNPs. A g-C<sub>3</sub>N<sub>4</sub>/PANI/PdNP nanohybrid composite modified electrodes by a simple one-step in situ electrochemical co-deposition method. Commonly, metallic Pd is an operative material for methanol electro-oxidation reactions. The results show two different oxidation waves for absorbed and adsorbed hydrogen above Pd [173].

As we know, redox reactions are responsible for energy storage at the electrode surface in supercapacitors. Thus, all efforts have been made to improve electrodes' efficiency performance in chemical stability and conductivity for energy storage [181]. Jose et al. illustrated a technique for the combination of palladium oxide-polypyrrole (PdP) with graphene oxide (rGO) to produce a PdPGO ternary to enhance electrochemical properties and increase stability. PdPGO has proven its efficiency in improving energy storage due to the individual properties of Pd NPs. Pd NPs are used in the synthesis of new materials for electrodes of supercapacitors to become high-efficiency and enhance high storage capability [174].

On the other hand, Fuku et al. reported producing H<sub>2</sub>O<sub>2</sub> from O<sub>2</sub> over Pd nanoparticle (NP) co-catalysts supported by BiVO<sub>4</sub> (cf. Figure 6). Accordingly, the performance of Pd NPs was optimal due to low overpotential and high selectivity for the two-electron reduction of O<sub>2</sub> [175].

#### 4.3. Pd Nanocatalyst for Hydrogenation Reactions

In general, traditional heterogeneous catalysts have low selectivity due to overhydrogenation. Usually, hydrogenation reactions occur under high temperatures and pressure so they become more dangerous; in contrast, if a Pd catalyst is used, the reaction occurs at room temperature and atmospheric pressure owing to the unique properties of Pd [182]. To increase the activity sites and surface area, there is an orientation toward using palladium nanoparticles [183].

More recently, researchers have been developing Pd NPs by merging with different ligands to raise the selectivity of organic reactions (cf. Table 3). Notable features of supported palladium nanoparticles are high efficiency, selectivity, and faster rate of reactions [184].

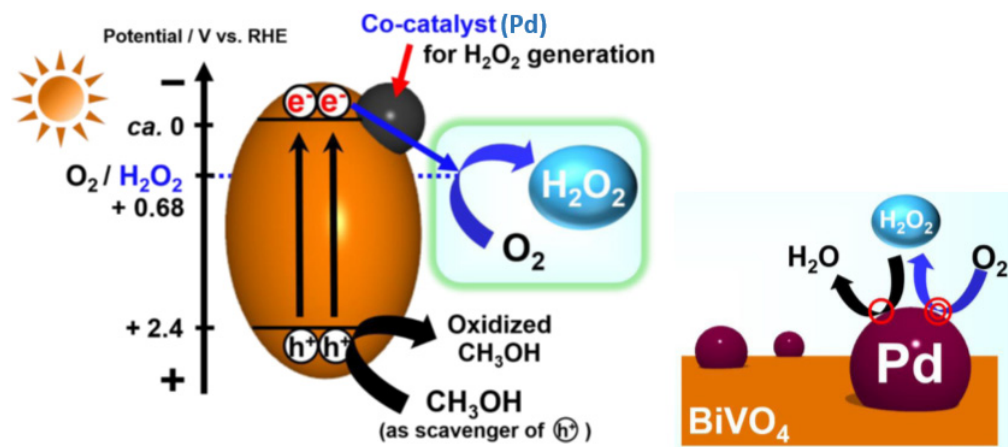


**Figure 6.** Schematic illustration of photocatalytic  $\text{H}_2\text{O}_2$  generation from  $\text{O}_2$  over a reductive co-catalyst supported  $\text{BiVO}_4$  in the presence of  $\text{CH}_3\text{OH}$  as a hole scavenger [175].

Advani et al. succeeded in preparing Pd NPs on N-doped graphitic carbon (N-C), starting from chitosan by carbonizing a Pd-chitosan complex under nitrogen atmosphere and high temperature. The Pd@N-C nanocatalyst was used to hydrogenate styrene to ethylbenzene; the result was excellent, as the conversion exceeded 99% with high selectivity. Furthermore, the Pd@N-C nanocatalyst was studied for hydrogenation of phenylacetylene and phenethyl alcohol; the results were that the conversion and selectivity were very high compared with other catalysts due to the nature of the strong interaction between Pd nanoparticles and graphitic/pyridinic N, where the electrons transferred from N-doped carbon towards the palladium nanoparticles led to an increase in the density of electrons, thus increasing the catalytic activity [185].

Pisarenko et al. studied the methylacetylene hydrogenation reaction in propane-propylene gas mixtures and used a Pd nanocatalyst ( $\text{Pd}/\alpha\text{-Al}_2\text{O}_3$ ) as a catalyst to obtain pure propylene [186].

The chemical industry is generally interested in the semi-hydrogenation of alkynes to alkenes, while alkane is unfavorable. The type of catalyst is important in semi-hydrogenation reactions because traditional catalysts reach over-hydrogenation, so the Pd nanocatalyst is high-efficiency selective of semi-hydrogenation and avoids over-hydrogenation [187]. Lv et al. prepared a meso-PdP nanocatalyst to convert 1-phenyl-1-propyne to propenyl benzene (cf. Figure 7). The result was the high performance of the conversion of 100% and a selectivity of 97.9% (95.9% cis-propenylbenzene). Owing to this, Pd is electrophilic and has an unfilled d-electron orbital, so drawing the electrons from P (nucleophilic) causes an increase in the density of electrons around Pd, thus increasing activity. Furthermore, the existence of mesoporous channels led to weakening of the adsorption and binding strengths of propenylbenzene on Pd-active sites, thus forbidding over-hydrogenation of propenylbenzene to phenylpropane [188].

**Table 3.** Different Pd nanocatalysts for hydrogenation reactions.

Catalyst	Product	Catalyst Loading	Temp	Time	Yield %	Ref.
Pd@N-C	ethylbenzene	50 mg	30 °C	-	>99	[185]
$\text{Pd}/\alpha\text{-Al}_2\text{O}_3$	propylene	0.05 wt% of Pd	120 °C	30 s	95	[186]
meso-PdP	propenylbenzene	-	-	60 min	100	[188]

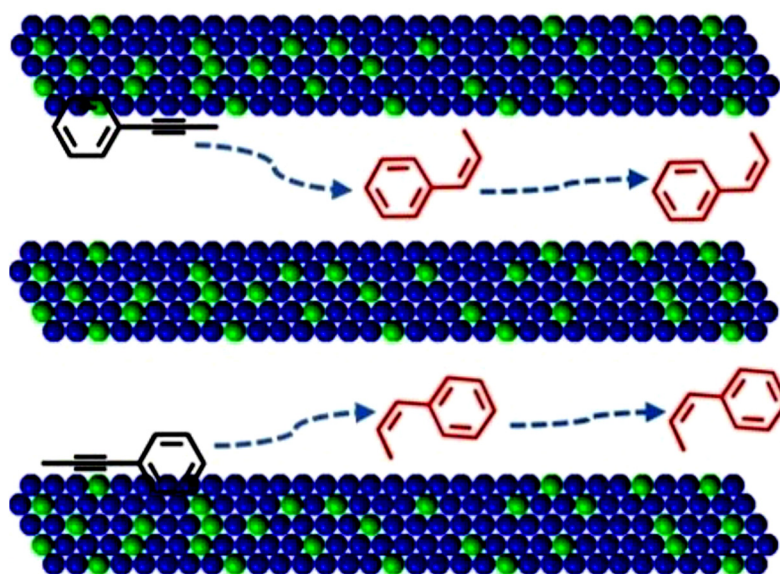


**Figure 7.** Schematic illustration of hydrogenation routes of 1-phenyl-1-propyne over meso-PdP nanobundles [188].

Fing et al. successfully synthesized PEI-Pd hydrogel by reacting 1-ethyl-3-(3-dimethylaminopropyl)carbodiimide-N-hydroxysuccinimide with palladium chloride solution to form metal-loaded composite hydrogels. PEI-Pd was used for the reduction of 4-nitrophenols (4-NP) to form 4-aminophenols (4-AP) in sewage (cf. Figure 8) [158]. Zhang and co-workers synthesized a novel bifunctional nanocatalyst with combined 3D acroscopic carbon nanotube (CNT)-graphene hydrogel (GH)-supported palladium NPs (Pd-CNT-GH), which is utilized for the catalytic reduction of 4-NP to 4-AP [159].

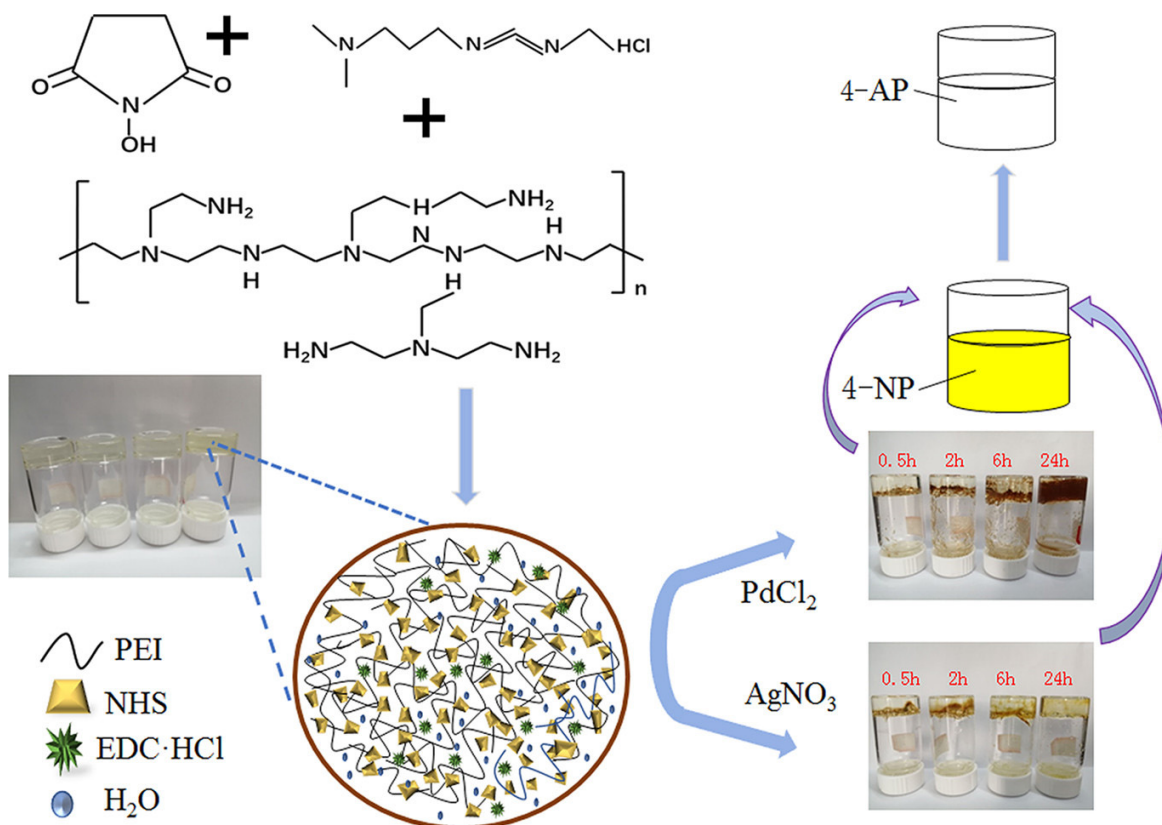


**Figure 8.** Synthesis and catalytic process of PEI hydrogel and PEI-Ag/PEI-Pd composites [158].

## 5. Medicinal Application of Pd NPs

Researchers have discovered the effects of Pd NPs in photothermal, anticancer, and antibacterial applications. Thus, using Pd NPs improves wound-healing properties and antimicrobial, anticancer, and antioxidant properties (cf. Table 4). Unfortunately, there are not a lot of research studies about Pd NPs in the biomedical field. In general, metal nanoparticles are considered one of the most powerful antibacterial agents, and this strength comes from their thermal flexibility and their ability to act on multidrug-resistant microorganisms [189].

**Table 4.** Different Pd nanocatalysts reported for their biomedical application.

Catalyst	Application	Catalyst Loading	Temp	Time	Yield %	Ref.
microbial Pd-NPs	Kill <i>Staphylococcus aureus</i> and <i>Escherichia coli</i>	20 mg/L	37 °C	10 min	99.99	[190]
PdNPs/GDY	Destroy cancer cells	-	-	-	50	[191]
PdNPs/GDY combine DOX	Destroy cancer cells	-	-	-	82.9	[191]
PVP-PdNPs	Breast cancer	10 µg/mL	37 °C	24 h	92	[192]

### 5.1. Pd NPs for Antibacterial Studies

Interestingly, antibacterial activity depends on the size and shape of Pd NPs. Some research illustrates that the larger size of Pd NPs has a lower effect in destroying *E. coli* than the smaller size. On the other hand, ultra-fine Pd NPs have vigorous activity in antimicrobial applications. In this regard, cubes and octahedrons of Pd nanocrystals are used to study the effect against Gram-negative and Gram-positive bacteria. Strikingly, the performance of Pd cubes with facets in destroying Gram-positive bacteria was more efficient compared with Pd octahedrons with facets; in contrast, the effect of Pd octahedrons with facets on Gram-negative bacteria was better efficient compared with Pd nanocubes [193].

The properties of Pd nanocrystals' oxidase and peroxidase activities have improved antibacterial activity's efficiency by producing reactive oxygen species (ROS). The way that Pd NPs damage microbes produces reactive oxygen species (ROS), causing harm to DNA and cell membranes and damage to proteins after destroying the electron transport system [194].

Some methods to kill bacteria depend on heat by converting near-infrared (NIR) light to heat, such as photothermal therapy (PTT), where PTT is an efficient and intact technique to transact with bacterial infections. Chen et al. used eco-friendly methods to prepare microbial Pd NPs by *Bacillus megatherium* Y-4 (cf. Figure 9). The cytotoxicity of microbial Pd NPs was investigated, where the result for microbial Pd NPs exhibited excellent biocompatibility. Also, it showed high antibacterial activity under NIR irradiation, where a low dose of Pd NPs (20 mg/L) was used to kill *Staphylococcus aureus* and *Escherichia coli*; during 10 min, 99.99% of bacteria were destroyed. Thus, Pd NPs can be used in PTT as an agent for fast sterilization applications due to Pd NPs having an efficient photothermal conversion ability [190].

In recent years, new methods have proven efficient in synthesizing nanoparticles with different shapes and sizes and have proven eco-friendly, such as the pulsed laser ablation in a liquid medium technique (PLAL). This technology inexpensively produces high-purity materials that depend on producing high-intensity pulses on a liquid material's surface [195]. Salman et al. successfully prepared Pd NPs using pulsed laser ablation with the liquid medium technique (PLAL). The study used Gram-positive (*Staphylococcus aureus*) and Gram-negative (*Escherichia coli*) bacteria to investigate the effectiveness of Pd NPs for antibacterial activity. Consequently, the performance of Pd NPs appeared to be more efficient in destroying Gram-negative bacteria than Gram-positive [196].

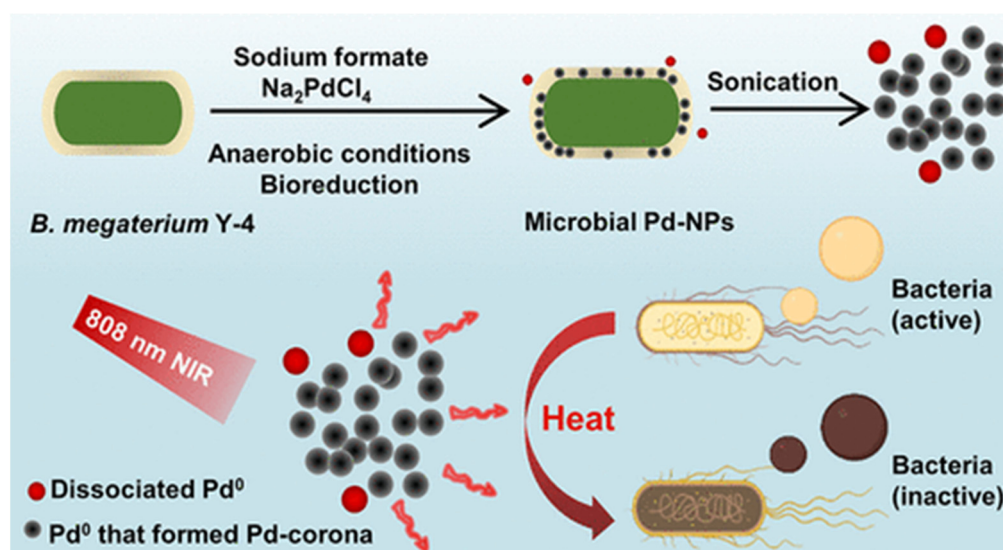


Figure 9. Schematic illustration of synthesis of microbial Pd NPs by *Bacillus megatherium* Y-4 [190].

### 5.2. Pd NPs for Anticancer Studies

The unique properties of Pd NPs show them to be strong candidates for cancer treatment with the photothermal method because they have strong absorption in the NIR region, photostability, high photothermal conversion efficiency, biocompatibility, and different sizes and shapes depending on the synthesis route [197].

In this regard, many researchers have illustrated Pd NPs' mechanism for damaging cancer cells. According to literature reports, Pd NPs bond with nitrogen bases and phosphate groups of DNA and protein where the bonding is physicochemical, inhibiting their activity. Lactate dehydrogenase (LDH) is important for producing cellular energy; however, Pd NPs cause the leakage of LDH, thus having an effect on the activity of cancer cells. Moreover, Pd NPs produce free radicals of ROS and reactive nitrogen species (RNS), which damages the composition of lipids of cancer cells [45].

The leading cause of the quick proliferation of cancer cells is hypoxia, because hypoxia activates HIF-1 (a dimeric protein complex) that controls tumorigenesis and progression. In general, cancer cells produce a large concentration of  $\text{H}_2\text{O}_2$ . Therefore, the target of researchers is to raise the concentration of  $\text{O}_2$  by decomposing the  $\text{H}_2\text{O}_2$  produced by neoplastic cells, inhibiting the HIF-1 level and avoiding the pervasion of neoplastic cells. Liu et al. synthesized a two-dimensional (2D) nanocatalyst, including Pd NPs immobilizing on graphdiyne's surface (GDY) (cf. Figure 10). PdNPs/GDY play the role of oxygen generator by decomposing  $\text{H}_2\text{O}_2$  into oxygen molecules inside cancer cells, thus preventing the rapid proliferation of neoplastic cells. The results proved that the efficiency of the antitumor effect was increased with the combination of PdNPs/GDY with a chemotherapeutic agent like doxorubicin (DOX) [191].

Breast cancer is a common cancer type in women, and it is regarded as curable in the premature stage of diagnosis. Ramalingam et al. successfully prepared PVP-PdNPs where polyvinylpyrrolidone (PVP) was immobilized on the surface of PdNPs utilizing an in situ single-step method. Moreover, the stability of PVP-PdNPs was proven due to the gain of Pd ions from pairs of electrons from the nitrogen or carbonyl oxygen of PVP. The performance of PVP-PdNPs was investigated by its anticancer activity against human breast cancer MCF7. Accordingly, PVP-PdNPs efficiently treated breast cancer MCF7 and had less cytotoxic activity against normal cells [192].

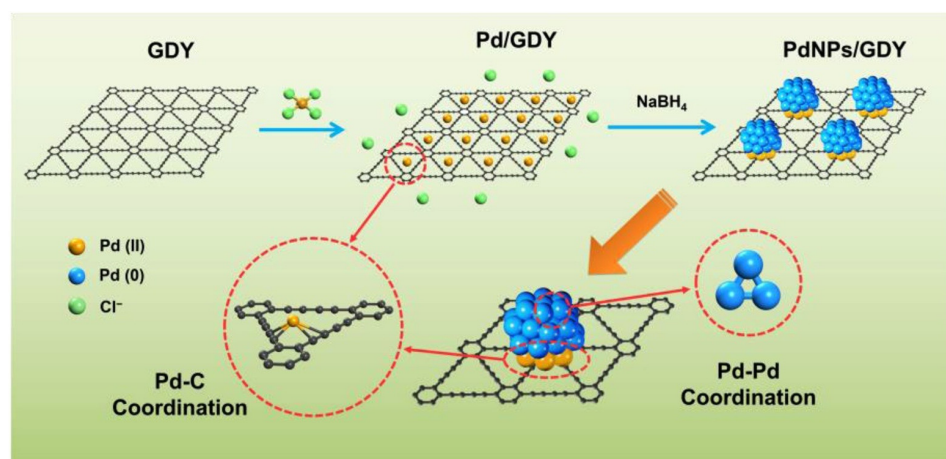


**Figure 10.** Schematic illustrations showing the synthesis of Pd/GDY and PdNPs/GDY [191].

## 6. Energy-Related Applications of Pd NPs

Apart from the studies reported above, there are a plethora of reports with regards to the energy-related applications of Pd NPs such as fuel cells, solar cells, and hydrogen production and storage.

In a recent study, E. Mari et al. demonstrated the use of flower-like graphitic carbon nitride/iron oxide/palladium nanocomposite for the electro-catalytic oxidation of ethylene glycol as a useful technique for preparing fuel cells. The authors detailed the fabrication of a  $g\text{-C}_3\text{N}_4/\text{Fe}_2\text{O}_3/\text{PdNPs}/\text{SPE}$  nanocomposite-modified electrode by the electrochemical deposition method for ethylene glycol oxidation [198]. The proposed  $g\text{-C}_3\text{N}_4/\text{Fe}_2\text{O}_3/\text{Pd}$  NPs nanocomposite has exceptional electro-oxidation efficiency while being highly durable compared to commercial Pd/C and other recently reported electro-catalyst materials. Therefore, it is a competent electro-catalyst for direct alcohol-based fuel cell applications (cf. Figure 11). The nanocomposite was found to be highly suitable for direct alcohol fuel cell applications, specifically for the electro-catalytic oxidation of ethylene glycol.

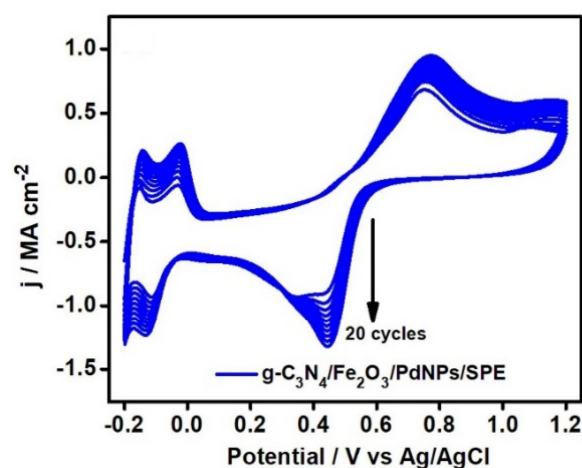


**Figure 11.** CV response of  $g\text{-C}_3\text{N}_4/\text{Fe}_2\text{O}_3/\text{PdNPs}$  nanocomposite electrodeposition in 1 mg/mL  $g\text{-C}_3\text{N}_4$ , 0.01 M  $\text{Fe}_2\text{O}_3$ , 0.005 M  $\text{PdCl}_2$ , and 0.5 M  $\text{H}_2\text{SO}_4$  at a sweep rate of  $20 \text{ mV s}^{-1}$  [198].

In another study, M.U. Rahman et al. developed an efficient and cost-effective counter electrode using 20 wt% of Pd NPs decorated on nitrogen-doped acetylene carbon black as dye-sensitized solar cells (DSSCs). The goal was to achieve higher power conversion efficiency and improve the overall performance of DSSCs. The outcomes showed that NCB@Pd displayed higher catalytic activity and efficiency compared to Pt, which was attributed to the nitrogen functional groups in the NCB support that modify the electronic

structure of Pd, as well as the smaller particle size of Pd NPs with better dispersion, which provided improved electrolyte diffusability due to more active sites for redox reactions. Additionally, the support played a role. The results obtained are presented in Figure 12. Overall, the study highlighted the potential of NCB@Pd as an alternative CE material for DSSCs [199].

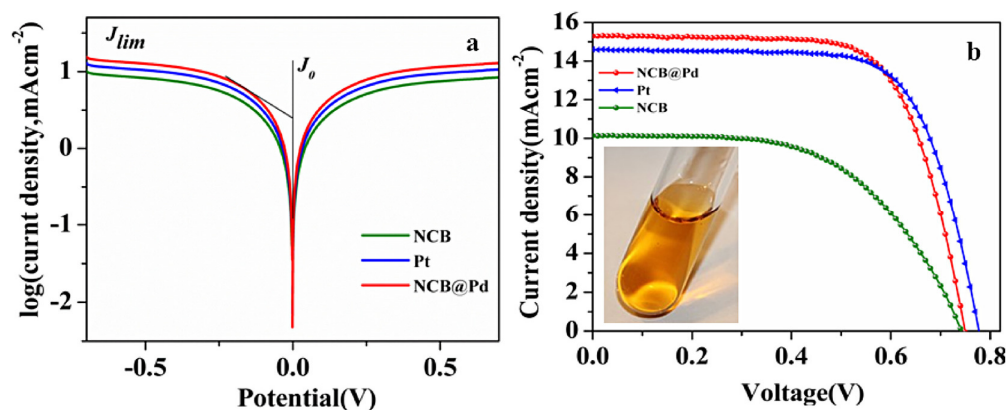


**Figure 12.** (a) Tafel polarization curves and (b) I–V curves of the DSSC with different counter electrodes [199].

Further work published by B.P. Vinayan et al. reported the synthesis of triangular-shaped Pd NP-decorated nitrogen-doped graphene, which was tested for its use as fuel cells and in hydrogen storage applications [200]. The study revealed that the as-prepared Pd/N-G exhibited higher hydrogen storage capacity compared to pure Pd nanoparticles, indicating the effectiveness of the spillover mechanism (cf. Figure 13).

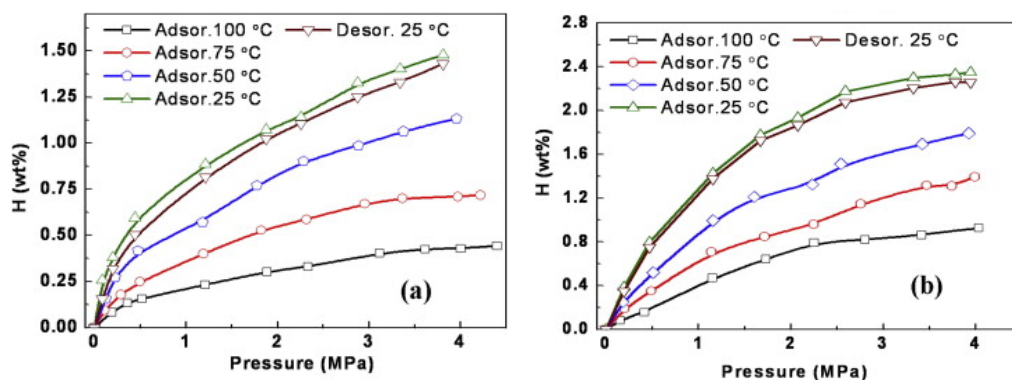


**Figure 13.** Hydrogen pressure-composition isotherms of (a) N-G and (b) Pd/N-G taken in the temperature range of 25–100 °C and pressure range of 0.1–4 MPa [200].

Another report by Kevin Dal Pont et al. [20] reported the preparation of Pd-based nanocomposites with a polyether block amide copolymer matrix while varying the percentage of Pd NPs. The nanocomposite with up to 20% Pd-based doping exhibited a typical response corresponding to ionic conductivity, with a decrease in  $\sigma'$  detected in the low-frequency spectral region. The pure polymer possessed conductivity of  $5.1 \times 10^{-9}$  S/cm; however, an increase in ionic conductivity was observed with an increase in doping of Pd NPs in the matrix [201].

Another research team, A.F. Oliveira et al., carried out some interesting work on the synthesis of palladium-doped titanium dioxide nanoparticles and their characterization for solar cell applications [202]. The reverse micelle sol-gel method was employed for synthesis of  $\text{TiO}_2$  and  $\text{TiO}_2$ :Pd (i.e., doped with Pd), which yielded a satisfactory yield of between 80 and 90% for the synthesis of pure  $\text{TiO}_2$  with various palladium dopings. The samples were subjected to impedance spectroscopy; from transmittance measurements employing

Tauc plot fittings, the optical energy gap was established, which revealed that almost all the samples possessed good ionic conductivity (cf. Figure 14).

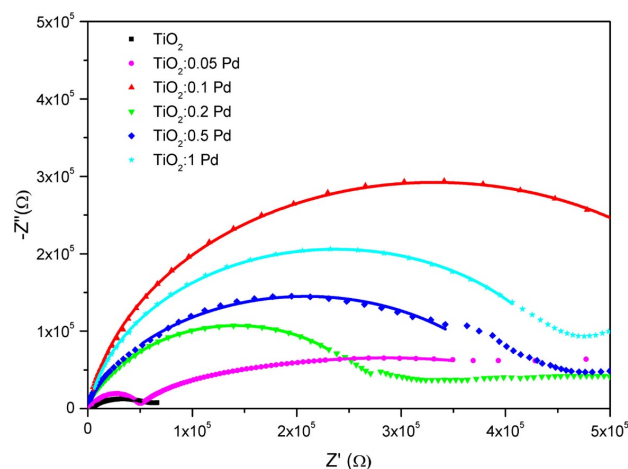


**Figure 14.** Impedance spectroscopy of  $\text{TiO}_2$  samples containing different Pd dopings after being kept under deionized water for 24 h [202].

## 7. Synthesis of Pd NPs

Lastly, we would like to mention briefly the synthesis of Pd NPs. There are several approaches which include physical and chemical methods. The physical methods with which Pd NPs have been reportedly synthesized are magnetron sputtering [203,204] and laser ablation [205,206], while chemical methods comprise electrochemical deposition [207], sonochemical methods [208–210], and supercritical fluid nucleation [211–213]. Moreover, Pd NPs have also been extensively synthesized by biogenic methods such as the use of plant-based extracts as reducing/stabilizing agents for their preparation, i.e., *Pulicaria glutinosa* extract, *Origanum vulgare* L. extract, *Syzygium aromaticum* aqueous extracts, *Filicium decipiens* leaf extract, *Santalum album* leaf extract, dried leaf of *Anacardium occidentale*, etc., which yielded a variety of Pd NPs with varying sizes and shapes [48,214–218]. In addition to this, microbial-mediated synthesis using bacteria, fungi, algae, and yeast has also been successfully attempted [30,219–222].

## 8. Conclusions

This review presents the latest literature study with regards to the applications of Pd NPs as sensors and catalysts and energy-related usage such as fuel cells and solar cells. Brief information about the medicinal applications of Pd NPs along with their uses in environmental remediation studies is also included. The sensor-related applications of Pd NPs have been extensively studied, and the performance efficiency has been enhanced by including another metal/metal oxide component along with the Pd NPs. However, there is scope to improve sensor-based activity by including newer 2D materials as supports which can be taken up by upcoming researchers. Moreover, the involvement of Pd NPs in organic conversion reactions as catalysts is also significantly investigated, and it has been found that they can be employed in various conversion reactions as well in the form of complexes with ligands to yield enantiomerically pure product. The medicinal uses of Pd NPs are mostly focused on antibacterial and anticancer applications, but their potential applications for various other ailments can be studied. With regards to environmental redemption and energy-related applications, there is still extensive scope for further study, which can be taken up by future researchers, such as the effect of various competitive impurities and the possibility of the leaching of Pd NPs while being used as an environmental redemption agent.

**Funding:** This research received no external funding.

**Data Availability Statement:** Not applicable.

**Conflicts of Interest:** The authors declare no conflict of interest.

## Abbreviations

TMNPs	transition metal nanoparticles
Pd NPs	palladium nanoparticles
Pd NWs	Pd nanowires
Pd NBRs	Pd broccolis
Pd NRs	Pd nanorods
PEI	polyethylenimine
4-NP	4-nitrophenols
4-AP	4-aminophenols
CNT	carbon nanotube
GH	graphene hydrogel
Cr(VI)	hexavalent chromium
FA	formic acid
MOFs	organic frameworks
SM	Suzuki-Miyaura cross-coupling
PdP	oxide-polypyrrole
rGO	graphene oxide
N-C	N-doped graphitic carbon
ROS	reactive oxygen species
NIR	near-infrared
PTT	photothermal therapy
PLAL	pulsed laser ablation in liquid medium technique
<i>E. coli</i>	<i>Escherichia coli</i>
LDH	lactate dehydrogenase
RNS	reactive nitrogen species
GDY	graphdiyne's surface
DOX	doxorubicin
PVP	polyvinylpyrrolidone
RT	room temperature
LSPR	localized surface plasmon resonance
Pd-Ag	palladium-silver
GOR	glucose oxidation reaction
VOCs	volatile organic compounds
HPC	hydroxypropyl cellulose
SWCNTs	single and multiwalled carbon nanotubes
PACs	porous activated carbons
SWASV	square-wave anodic voltammetry
SWCNT	single-walled carbon nanotube
FET	field-effect transistor
CAP	chloramphenicol
rGO-PdNP	Pd NP-decorated highly reduced graphene oxide
AA	ascorbic acid
SAW	surface acoustic wave
DSSCs	dye-sensitized solar cells

## References

- Shubha, J.P.; Savitha, H.S.; Patil, R.C.; Assal, M.E.; Shaik, M.R.; Kuniyil, M.; Alduhaish, O.; Dubasi, N.; Farooq Adil, S. A green approach for the degradation of toxic textile dyes by nickel oxide (NiO-SD) NPs: Photocatalytic and kinetic approach. *J. King Saud Univ.-Sci.* **2023**, *35*, 102784. [[CrossRef](#)]
- Al-Janabi, A.S.M.; Oudah, K.H.; Aldossari, S.A.; Khalaf, M.A.; Saleh, A.M.; Hatshan, M.R.; Altheeb, N.B.; Farooq Adil, S. Spectroscopic, anti-bacterial, anti-cancer and molecular docking of Pd(II) and Pt(II) complexes with (E)-4-((dimethylamino)methyl)-2-((4,5-dimethylthiazol-2-yl)diazanyl)phenol ligand. *J. Saudi Chem. Soc.* **2023**, *27*, 101619. [[CrossRef](#)]

3. Albano, G.; Petri, A.; Aronica, L.A. Palladium Supported on Bioinspired Materials as Catalysts for C-C Coupling Reactions. *Catalysts* **2023**, *13*, 210. [[CrossRef](#)]
4. Shaik, M.R.; Khan, M.; Kumar, J.V.S.; Ashraf, M.; Khan, M.; Kuniyil, M.; Assal, M.E.; Al-Warthan, A.; Siddiqui, M.R.H.; Khan, A.; et al. Nano Nickel-Zirconia: An Effective Catalyst for the Production of Biodiesel from Waste Cooking Oil. *Crystals* **2023**, *13*, 592. [[CrossRef](#)]
5. Almutairi, E.M.; Ghanem, M.A.; Al-Warthan, A.; Kuniyil, M.; Adil, S.F. Hydrazine High-Performance Oxidation and Sensing Using a Copper Oxide Nanosheet Electrocatalyst Prepared via a Foam-Surfactant Dual Template. *Nanomaterials* **2023**, *13*, 129. [[CrossRef](#)]
6. Kumar, K.P.A.; Alduhaish, O.; Adil, S.F.; Pumera, M. Grafting of Pd on Covalently and Noncovalently Modified N-Doped Graphene for Electrocatalysis. *Adv. Mater. Interfaces* **2022**, *9*, 2102317. [[CrossRef](#)]
7. Shubha, J.P.; Kavalli, K.; Adil, S.F.; Assal, M.E.; Hatshan, M.R.; Dubasi, N. Facile green synthesis of semiconductive ZnO nanoparticles for photocatalytic degradation of dyes from the textile industry: A kinetic approach. *J. King Saud Univ.-Sci.* **2022**, *34*, 102047. [[CrossRef](#)]
8. Khan, M.; Ashraf, M.; Shaik, M.R.; Adil, S.F.; Islam, M.S.; Kuniyil, M.; Khan, M.; Hatshan, M.R.; Alshammari, R.H.; Siddiqui, M.R.H.; et al. Pyrene Functionalized Highly Reduced Graphene Oxide-palladium Nanocomposite: A Novel Catalyst for the Mizoroki-Heck Reaction in Water. *Front. Chem.* **2022**, *10*, 872366. [[CrossRef](#)]
9. Ibrahim, A.A.; Fakeeha, A.H.; Lanre, M.S.; Al-Awadi, A.S.; Alreshaidan, S.B.; Albaqmaa, Y.A.; Adil, S.F.; Al-Zahrani, A.A.; Abasaed, A.E.; Al-Fatesh, A.S. The Effect of Calcination Temperature on Various Sources of ZrO<sub>2</sub> Supported Ni Catalyst for Dry Reforming of Methane. *Catalysts* **2022**, *12*, 361. [[CrossRef](#)]
10. Zhang, M.; Wang, L.; Yan, H.; Lian, L.; Si, J.; Long, Z.; Cui, X.; Wang, J.; Zhao, L.; Yang, C. Palladium-halloysite nanocomposites as an efficient heterogeneous catalyst for acetylene hydrochlorination. *J. Mater. Res. Technol.* **2021**, *13*, 2055–2065. [[CrossRef](#)]
11. Khan, M.; Karuppiyah, P.; Alkhathlan, H.Z.; Kuniyil, M.; Khan, M.; Adil, S.F.; Shaik, M.R. Green Synthesis of Silver Nanoparticles Using *Juniperus procera* Extract: Their Characterization, and Biological Activity. *Crystals* **2022**, *12*, 420. [[CrossRef](#)]
12. Khan, M.; Al-Hamoud, K.; Liaqat, Z.; Shaik, M.R.; Adil, S.F.; Kuniyil, M.; Alkhathlan, H.Z.; Al-Warthan, A.; Siddiqui, M.R.H.; Mondeshki, M.; et al. Synthesis of Au, Ag, and Au-Ag Bimetallic Nanoparticles Using *Pulicaria undulata* Extract and Their Catalytic Activity for the Reduction of 4-Nitrophenol. *Nanomaterials* **2020**, *10*, 1885. [[CrossRef](#)] [[PubMed](#)]
13. Joudeh, N.; Saragliadis, A.; Koster, G.; Mikheenko, P.; Linke, D. Synthesis methods and applications of palladium nanoparticles: A review. *Front. Nanotechnol.* **2022**, *4*, 1062608. [[CrossRef](#)]
14. Chen, S.; Wang, G.; Sui, W.; Parvez, A.M.; Dai, L.; Si, C. Novel lignin-based phenolic nanosphere supported palladium nanoparticles with highly efficient catalytic performance and good reusability. *Ind. Crops Prod.* **2020**, *145*, 112164. [[CrossRef](#)]
15. Yurkov, G.; Koksharov, Y.; Fionov, A.; Taratanov, N.; Kolesov, V.; Kirillov, V.; Makeev, M.; Mikhalev, P.; Ryzhenko, D.; Solodilov, V. Polymer Nanocomposite Containing Palladium Nanoparticles: Synthesis, Characterization, and Properties. *Polymers* **2022**, *14*, 3795. [[CrossRef](#)]
16. Favier, I.; Pla, D.; Gómez, M. Palladium nanoparticles in polyols: Synthesis, catalytic couplings, and hydrogenations. *Chem. Rev.* **2019**, *120*, 1146–1183. [[CrossRef](#)]
17. Thirumalraj, B.; Rajkumar, C.; Chen, S.-M.; Veerakumar, P.; Perumal, P.; Liu, S.-B. Carbon aerogel supported palladium-ruthenium nanoparticles for electrochemical sensing and catalytic reduction of food dye. *Sens. Actuators B Chem.* **2018**, *257*, 48–59. [[CrossRef](#)]
18. Jameel, M.S.; Aziz, A.A.; Dheyab, M.A.; Mehrdel, B.; Khaniabadi, P.M. Rapid sonochemically-assisted green synthesis of highly stable and biocompatible platinum nanoparticles. *Surf. Interfaces* **2020**, *20*, 100635. [[CrossRef](#)]
19. Oshima, K.; Shiraiishi, Y.; Matsumura, T.; Kuriyama, A.; Taguchi, K.; Inoue, J.; Anno, H.; Toshima, N. Enhancement of the electrical conductivity of defective carbon nanotube sheets for organic hybrid thermoelectrics by deposition of Pd nanoparticles. *Mater. Adv.* **2020**, *1*, 2926–2936. [[CrossRef](#)]
20. Fahmy, S.A.; Preis, E.; Bakowsky, U.; Azzazy, H.M.E.-S. Palladium nanoparticles fabricated by green chemistry: Promising chemotherapeutic, antioxidant and antimicrobial agents. *Materials* **2020**, *13*, 3661. [[CrossRef](#)]
21. Dong, M.; Qian, W.; Liu, X.; Chen, Y.; Huang, W.; Dong, C. Enhanced thermo cell properties from N-doped carbon nanotube-Pd composite electrode. *Surf. Coat. Technol.* **2022**, *434*, 128213. [[CrossRef](#)]
22. Sikeyi, L.L.; Matthews, T.; Adekunle, A.S.; Maxakato, N.W. Electro-oxidation of Ethanol and Methanol on Pd/C, Pd/CNFs and Pd-Ru/CNFs Nanocatalysts in Alkaline Direct Alcohol Fuel Cell. *Electroanalysis* **2020**, *32*, 2681–2692. [[CrossRef](#)]
23. Fernández-Arias, M.; Vilas, A.M.; Boutinguiza, M.; Rodríguez, D.; Arias-González, F.; Pou-Álvarez, P.; Riveiro, A.; Gil, J.; Pou, J. Palladium nanoparticles synthesized by laser ablation in liquids for antimicrobial applications. *Nanomaterials* **2022**, *12*, 2621. [[CrossRef](#)] [[PubMed](#)]
24. Osonga, F.J.; Kalra, S.; Miller, R.M.; Isika, D.; Sadik, O.A. Synthesis, characterization and antifungal activities of eco-friendly palladium nanoparticles. *RSC Adv.* **2020**, *10*, 5894–5904. [[CrossRef](#)]
25. Ali, S.; Sharma, A.S.; Ahmad, W.; Zareef, M.; Hassan, M.M.; Viswadevarayalu, A.; Jiao, T.; Li, H.; Chen, Q. Noble metals based bimetallic and trimetallic nanoparticles: Controlled synthesis, antimicrobial and anticancer applications. *Crit. Rev. Anal. Chem.* **2021**, *51*, 454–481. [[CrossRef](#)]
26. Xu, Y.; Musumeci, V.; Aymonier, C. Chemistry in supercritical fluids for the synthesis of metal nanomaterials. *React. Chem. Eng.* **2019**, *4*, 2030–2054. [[CrossRef](#)]

27. Wang, H.; Zhao, W.; Zhao, Y.; Xu, C.-H.; Xu, J.-J.; Chen, H.-Y. Real-time tracking the electrochemical synthesis of Au@metal core-shell nanoparticles toward photo enhanced methanol oxidation. *Anal. Chem.* **2020**, *92*, 14006–14011. [[CrossRef](#)]
28. Yu, Y.; Theerthagiri, J.; Lee, S.J.; Muthusamy, G.; Ashokkumar, M.; Choi, M.Y. Integrated technique of pulsed laser irradiation and sonochemical processes for the production of highly surface-active NiPd spheres. *Chem. Eng. J.* **2021**, *411*, 128486. [[CrossRef](#)]
29. Guo, J.; Liu, W.; Fu, X.-C.; Jiao, S. Wet-chemistry synthesis of two-dimensional Pt-and Pd-based intermetallic electrocatalysts for fuel cells. *Nanoscale* **2023**, *15*, 8508–8531. [[CrossRef](#)]
30. Mohana, S.; Sumathi, S. Multi-functional biological effects of palladium nanoparticles synthesized using *Agaricus bisporus*. *J. Clust. Sci.* **2020**, *31*, 391–400. [[CrossRef](#)]
31. Altuner, E.E.; Gulbagca, F.; Tiri, R.N.E.; Aygun, A.; Sen, F. Highly efficient palladium-zinc oxide nanoparticles synthesized by biogenic methods: Characterization, hydrogen production and photocatalytic activities. *Chem. Eng. J. Adv.* **2023**, *14*, 100465. [[CrossRef](#)]
32. Tan, K.B.; Sun, D.; Huang, J.; Odoom-Wubah, T.; Li, Q. State of arts on the bio-synthesis of noble metal nanoparticles and their biological application. *Chin. J. Chem. Eng.* **2021**, *30*, 272–290. [[CrossRef](#)]
33. Kaur, M.; Sharma, C.; Sharma, N.; Jamwal, B.; Paul, S. Pd Nanoparticles Decorated on ZnO/Fe<sub>3</sub>O<sub>4</sub> Cores and Doped with Mn<sup>2+</sup> and Mn<sup>3+</sup> for Catalytic C-C Coupling, Nitroaromatics Reduction, and the Oxidation of Alcohols and Hydrocarbons. *ACS Appl. Nano Mater.* **2020**, *3*, 10310–10325. [[CrossRef](#)]
34. Patnaik, S.; Sahoo, D.P.; Parida, K. Bimetallic co-effect of Au-Pd alloyed nanoparticles on mesoporous silica modified g-C<sub>3</sub>N<sub>4</sub> for single and simultaneous photocatalytic oxidation of phenol and reduction of hexavalent chromium. *J. Colloid Interface Sci.* **2020**, *560*, 519–535. [[CrossRef](#)] [[PubMed](#)]
35. Uegaki, N.; Seino, S.; Ohkubo, Y.; Nakagawa, T. Effect of Polymer Substrate on Adhesion of Electroless Plating in Irradiation-Based Direct Immobilization of Pd Nanoparticles Catalyst. *Nanomaterials* **2022**, *12*, 4106. [[CrossRef](#)]
36. Wei, Z.; Xie, Z.; Gao, L.; Wang, Y.; Sun, H.; Jian, Y.; Zhang, G.; Xu, L.; Yang, J.; Zhang, W. Highly crystallized Pd/Cu nanoparticles on activated carbon: An efficient heterogeneous catalyst for Sonogashira cross-coupling reaction. *Catalysts* **2020**, *10*, 192. [[CrossRef](#)]
37. Zhang, X.; Yang, P. Pd nanoparticles assembled on Ni- and N-doped carbon nanotubes towards superior electrochemical activity. *Int. J. Hydrogen Energy* **2021**, *46*, 2065–2074. [[CrossRef](#)]
38. Veerakumar, P.; Lin, K.-C. An overview of palladium supported on carbon-based materials: Synthesis, characterization, and its catalytic activity for reduction of hexavalent chromium. *Chemosphere* **2020**, *253*, 126750. [[CrossRef](#)]
39. Pei, A.; Ruan, L.; Liao, J.; Zhang, H.; Wang, J.; Yang, K.; Liu, Z.; Zhu, L.; Chen, B.H. Preparation of a PdRuNi/C tri-metallic nanocatalyst and its excellent catalytic performance for ethylbenzene hydrogenation reaction. *New J. Chem.* **2019**, *43*, 17306–17314. [[CrossRef](#)]
40. Liu, L.; Zhang, L.; Kim, S.M.; Park, S. Helical metallic micro-and nanostructures: Fabrication and application. *Nanoscale* **2014**, *6*, 9355–9365. [[CrossRef](#)]
41. Zheng, G.; Mourdikoudis, S.; Zhang, Z. Plasmonic metallic heteromeric nanostructures. *Small* **2020**, *16*, 2002588. [[CrossRef](#)] [[PubMed](#)]
42. Khurana, K.; Jaggi, N. Localized surface plasmonic properties of Au and Ag nanoparticles for sensors: A review. *Plasmonics* **2021**, *16*, 981–999. [[CrossRef](#)]
43. Zhang, Y.; Chu, W.; Foroushani, A.D.; Wang, H.; Li, D.; Liu, J.; Barrow, C.J.; Wang, X.; Yang, W. New gold nanostructures for sensor applications: A review. *Materials* **2014**, *7*, 5169–5201. [[CrossRef](#)] [[PubMed](#)]
44. Murphy, C.J.; Gole, A.M.; Hunyadi, S.E.; Stone, J.W.; Sisco, P.N.; Alkilany, A.; Kinard, B.E.; Hankins, P. Chemical sensing and imaging with metallic nanorods. *Chem. Commun.* **2008**, 544–557. [[CrossRef](#)] [[PubMed](#)]
45. Phan, T.T.V.; Huynh, T.-C.; Manivasagan, P.; Mondal, S.; Oh, J. An up-to-date review on biomedical applications of palladium nanoparticles. *Nanomaterials* **2019**, *10*, 66. [[CrossRef](#)]
46. Hong, K.; Sajjadi, M.; Suh, J.M.; Zhang, K.; Nasrollahzadeh, M.; Jang, H.W.; Varma, R.S.; Shokouhimehr, M. Palladium nanoparticles on assorted nanostructured supports: Applications for Suzuki, Heck, and Sonogashira cross-coupling reactions. *ACS Appl. Nano Mater.* **2020**, *3*, 2070–2103. [[CrossRef](#)]
47. Luo, S.; Zeng, Z.; Zeng, G.; Liu, Z.; Xiao, R.; Chen, M.; Tang, L.; Tang, W.; Lai, C.; Cheng, M. Metal organic frameworks as robust host of palladium nanoparticles in heterogeneous catalysis: Synthesis, application, and prospect. *ACS Appl. Mater. Interfaces* **2019**, *11*, 32579–32598. [[CrossRef](#)]
48. Khan, M.; Khan, M.; Kuniyil, M.; Adil, S.F.; Al-Warthan, A.; Alkhatlan, H.Z.; Tremel, W.; Tahir, M.N.; Siddiqui, M.R.H. Biogenic synthesis of palladium nanoparticles using *Pulicaria glutinosa* extract and their catalytic activity towards the Suzuki coupling reaction. *Dalton Trans.* **2014**, *43*, 9026–9031. [[CrossRef](#)]
49. Zhang, D.; Zheng, X.; Qi, L.; Xue, Y.; He, F.; Li, Y. Controlled growth of single-crystal Pd quantum dots on 2D carbon for large current density hydrogen evolution. *Adv. Funct. Mater.* **2022**, *32*, 2111501. [[CrossRef](#)]
50. Wang, Y.; Liu, J.; Yuan, H.; Liu, F.; Hu, T.; Yang, B. Strong Electronic Interaction between Amorphous MnO<sub>2</sub> Nanosheets and Ultrafine Pd Nanoparticles toward Enhanced Oxygen Reduction and Ethylene Glycol Oxidation Reactions. *Adv. Funct. Mater.* **2023**, *33*, 2211909. [[CrossRef](#)]
51. Kuniyil, M.; Kumar, J.S.; Adil, S.F.; Shaik, M.R.; Khan, M.; Assal, M.E.; Siddiqui, M.R.H.; Al-Warthan, A. One-pot synthesized Pd@N-doped graphene: An efficient catalyst for Suzuki-Miyaura couplings. *Catalysts* **2019**, *9*, 469. [[CrossRef](#)]

52. Khan, M.; Kuniyil, M.; Shaik, M.R.; Khan, M.; Adil, S.F.; Al-Warthan, A.; Alkhatlan, H.Z.; Tremel, W.; Tahir, M.N.; Siddiqui, M.R.H. Plant Extract Mediated Eco-Friendly Synthesis of Pd@Graphene Nanocatalyst: An Efficient and Reusable Catalyst for the Suzuki-Miyaura Coupling. *Catalysts* **2017**, *7*, 20. [[CrossRef](#)]
53. Chuentragool, P.; Kurandina, D.; Gevorgyan, V. Catalysis with palladium complexes photoexcited by visible light. *Angew. Chem. Int. Ed.* **2019**, *58*, 11586–11598. [[CrossRef](#)] [[PubMed](#)]
54. Kanwal, I.; Mujahid, A.; Rasool, N.; Rizwan, K.; Malik, A.; Ahmad, G.; Shah, S.A.A.; Rashid, U.; Nasir, N.M. Palladium and copper catalyzed Sonogashira cross coupling an excellent methodology for CC bond formation over 17 years: A review. *Catalysts* **2020**, *10*, 443. [[CrossRef](#)]
55. Antolini, E. Palladium in fuel cell catalysis. *Energy Environ. Sci.* **2009**, *2*, 915–931. [[CrossRef](#)]
56. Calderón Gómez, J.C.; Moliner, R.; Lázaro, M.J. Palladium-based catalysts as electrodes for direct methanol fuel cells: A last ten years review. *Catalysts* **2016**, *6*, 130. [[CrossRef](#)]
57. Konda, S.K.; Chen, A. Palladium based nanomaterials for enhanced hydrogen spillover and storage. *Mater. Today* **2016**, *19*, 100–108. [[CrossRef](#)]
58. Darmadi, I.; Nugroho, F.A.A.; Langhammer, C. High-performance nanostructured palladium-based hydrogen sensors—Current limitations and strategies for their mitigation. *ACS Sens.* **2020**, *5*, 3306–3327. [[CrossRef](#)]
59. Kumar, A.; Mohammadi, M.M.; Swihart, M.T. Synthesis, growth mechanisms, and applications of palladium-based nanowires and other one-dimensional nanostructures. *Nanoscale* **2019**, *11*, 19058–19085. [[CrossRef](#)]
60. Mirzaei, A.; Yousefi, H.R.; Falsafi, F.; Bonyani, M.; Lee, J.-H.; Kim, J.-H.; Kim, H.W.; Kim, S.S. An overview on how Pd on resistive-based nanomaterial gas sensors can enhance response toward hydrogen gas. *Int. J. Hydrogen Energy* **2019**, *44*, 20552–20571. [[CrossRef](#)]
61. Cao, P.; Yang, Z.; Navale, S.; Han, S.; Liu, X.; Liu, W.; Lu, Y.; Stadler, F.; Zhu, D. Ethanol sensing behavior of Pd-nanoparticles decorated ZnO-nanorod based chemiresistive gas sensors. *Sens. Actuators B Chem.* **2019**, *298*, 126850. [[CrossRef](#)]
62. Zhang, H.; Jin, M.; Xiong, Y.; Lim, B.; Xia, Y. Shape-controlled synthesis of Pd nanocrystals and their catalytic applications. *Acc. Chem. Res.* **2013**, *46*, 1783–1794. [[CrossRef](#)] [[PubMed](#)]
63. Xiong, Y.; Xia, Y. Shape-controlled synthesis of metal nanostructures: The case of palladium. *Adv. Mater.* **2007**, *19*, 3385–3391. [[CrossRef](#)]
64. Ananikov, V.P.; Orlov, N.V.; Beletskaya, I.P.; Khrustalev, V.N.; Antipin, M.Y.; Timofeeva, T.V. New approach for size-and shape-controlled preparation of Pd nanoparticles with organic ligands. Synthesis and application in catalysis. *J. Am. Chem. Soc.* **2007**, *129*, 7252–7253. [[CrossRef](#)]
65. Niu, W.; Zhang, L.; Xu, G. Shape-controlled synthesis of single-crystalline palladium nanocrystals. *Acs Nano* **2010**, *4*, 1987–1996. [[CrossRef](#)] [[PubMed](#)]
66. Bhardwaj, P.; Barman, P.B.; Hazra, S.K. Shape dependent hydrogen response in palladium nanoparticle based sensors. *Mater. Today Proc.* **2020**, *28*, 218–222. [[CrossRef](#)]
67. Sugawa, K.; Tahara, H.; Yamashita, A.; Otsuki, J.; Sagara, T.; Harumoto, T.; Yanagida, S. Refractive index susceptibility of the plasmonic palladium nanoparticle: Potential as the third plasmonic sensing material. *Acs Nano* **2015**, *9*, 1895–1904. [[CrossRef](#)]
68. De Marchi, S.; Núñez-Sánchez, S.; Bodelón, G.; Pérez-Juste, J.; Pastoriza-Santos, I. Pd nanoparticles as a plasmonic material: Synthesis, optical properties and applications. *Nanoscale* **2020**, *12*, 23424–23443. [[CrossRef](#)]
69. Tittel, A.; Mai, P.; Taubert, R.; Dregely, D.; Liu, N.; Giessen, H. Palladium-based plasmonic perfect absorber in the visible wavelength range and its application to hydrogen sensing. *Nano Lett.* **2011**, *11*, 4366–4369. [[CrossRef](#)]
70. Amirjani, A.; Amlashi, N.B.; Ahmadiani, Z.S. Plasmon-Enhanced Photocatalysis Based on Plasmonic Nanoparticles for Energy and Environmental Solutions: A Review. *ACS Appl. Nano Mater.* **2023**, *6*, 9085–9123. [[CrossRef](#)]
71. Langhammer, C.; Yuan, Z.; Zorić, I.; Kasemo, B. Plasmonic properties of supported Pt and Pd nanostructures. *Nano Lett.* **2006**, *6*, 833–838. [[CrossRef](#)] [[PubMed](#)]
72. Huang, X.; Tang, S.; Mu, X.; Dai, Y.; Chen, G.; Zhou, Z.; Ruan, F.; Yang, Z.; Zheng, N. Freestanding palladium nanosheets with plasmonic and catalytic properties. *Nat. Nanotechnol.* **2011**, *6*, 28–32. [[CrossRef](#)] [[PubMed](#)]
73. Mayer, K.M.; Hafner, J.H. Localized surface plasmon resonance sensors. *Chem. Rev.* **2011**, *111*, 3828–3857. [[CrossRef](#)] [[PubMed](#)]
74. Bartlett, P.N.; Guerin, S. A micromachined calorimetric gas sensor: An application of electrodeposited nanostructured palladium for the detection of combustible gases. *Anal. Chem.* **2003**, *75*, 126–132. [[CrossRef](#)] [[PubMed](#)]
75. Sakamoto, Y.; Chen, F.; Ura, M.; Flanagan, T. Thermodynamic Properties for Solution of Hydrogen in Palladium-Based Binary Alloys. *Berichte Bunsenges. Für Phys. Chem.* **1995**, *99*, 807–820. [[CrossRef](#)]
76. Chandrasekhar, N.; Sholl, D.S. Quantitative computational screening of Pd-based intermetallic membranes for hydrogen separation. *J. Membr. Sci.* **2014**, *453*, 516–524. [[CrossRef](#)]
77. Peng, L.; Rao, Y.; Luo, L.; Chen, C.A. The poisoning of Pd-Y alloy membranes by carbon monoxide. *J. Alloys Compd.* **2009**, *486*, 74–77. [[CrossRef](#)]
78. Alrammouz, R.; Podlecki, J.; Abboud, P.; Sorli, B.; Habchi, R. A review on flexible gas sensors: From materials to devices. *Sens. Actuators A Phys.* **2018**, *284*, 209–231. [[CrossRef](#)]
79. Cui, L.-J.; Shang, H.-C.; Zhang, G.; Li, Y.; Zhao, Z.-X. Experimental study on optical fiber bundle hydrogen sensor based on palladium-silver optical thin film. *Optoelectron. Lett.* **2013**, *9*, 13–17. [[CrossRef](#)]

80. Gutés, A.; Carraro, C.; Maboudian, R. Nonenzymatic glucose sensing based on deposited palladium nanoparticles on epoxy-silver electrodes. *Electrochim. Acta* **2011**, *56*, 5855–5859. [[CrossRef](#)]
81. Monzón-Hernández, D.; Luna-Moreno, D.; Martínez-Escobar, D. Fast response fiber optic hydrogen sensor based on palladium and gold nano-layers. *Sens. Actuators B Chem.* **2009**, *136*, 562–566. [[CrossRef](#)]
82. Strohfeldt, N.; Zhao, J.; Tittel, A.; Giessen, H. Sensitivity engineering in direct contact palladium-gold nano-sandwich hydrogen sensors. *Opt. Mater. Express* **2015**, *5*, 2525–2535. [[CrossRef](#)]
83. Singh, S.; Tripathi, P.; Kumar, N.; Nara, S. Colorimetric sensing of malathion using palladium-gold bimetallic nanozyme. *Biosens. Bioelectron.* **2017**, *92*, 280–286. [[CrossRef](#)] [[PubMed](#)]
84. Li, X.; Liu, Y.; Hemminger, J.C.; Penner, R.M. Catalytically activated palladium@platinum nanowires for accelerated hydrogen gas detection. *ACS Nano* **2015**, *9*, 3215–3225. [[CrossRef](#)] [[PubMed](#)]
85. Ye, J.-S.; Hong, B.-D.; Wu, Y.-S.; Chen, H.-R.; Lee, C.-L. Heterostructured palladium-platinum core-shell nanocubes for use in a nonenzymatic amperometric glucose sensor. *Microchim. Acta* **2016**, *183*, 3311–3320.
86. Andersson, J.; Svirelis, J.; Del Castillo, G.F.-D.; Sannomiya, T.; Dahlin, A. Surface plasmon resonance sensing with thin films of palladium and platinum-quantitative and real-time analysis. *Phys. Chem. Chem. Phys.* **2022**, *24*, 4588–4594. [[CrossRef](#)]
87. Yu, K.; Tian, X.; Wang, X.; Yang, F.; Qi, T.; Zuo, J. Enhanced accuracy of palladium-nickel alloy based hydrogen sensor by in situ temperature compensation. *Sens. Actuators B Chem.* **2019**, *299*, 126989. [[CrossRef](#)]
88. Zhao, D.; Xu, C. A nanoporous palladium-nickel alloy with high sensing performance towards hydrogen peroxide and glucose. *J. Colloid Interface Sci.* **2015**, *447*, 50–57. [[CrossRef](#)]
89. Wang, W.; Liu, X.; Mei, S.; Jia, Y.; Liu, M.; Xue, X.; Yang, D. Development of a Pd/Cu nanowires coated SAW hydrogen gas sensor with fast response and recovery. *Sens. Actuators B Chem.* **2019**, *287*, 157–164. [[CrossRef](#)]
90. Zou, C.e.; Zhong, J.; Wang, J.; Shiraishi, Y.; Li, S.; Yan, B.; Guo, J.; Du, Y. Fabrication of reduced graphene oxide-bimetallic Pd@Au nanocomposites for simultaneous determination of ascorbic acid, dopamine and uric acid. *RSC Adv.* **2016**, *6*, 92502–92509.
91. Ghosh, S.; RoyChaudhuri, C.; Bhattacharya, R.; Saha, H.; Mukherjee, N. Palladium-silver-activated ZnO surface: Highly selective methane sensor at reasonably low operating temperature. *ACS Appl. Mater. Interfaces* **2014**, *6*, 3879–3887. [[CrossRef](#)] [[PubMed](#)]
92. Sowmya, B.; John, A.; Panda, P. A review on metal-oxide based pn and nn heterostructured nano-materials for gas sensing applications. *Sens. Int.* **2021**, *2*, 100085.
93. Yang, S.; Lei, G.; Xu, H.; Lan, Z.; Wang, Z.; Gu, H. Metal oxide based heterojunctions for gas sensors: A review. *Nanomaterials* **2021**, *11*, 1026. [[CrossRef](#)]
94. Kumar, V.; Sen, S.; Muthe, K.; Gaur, N.; Gupta, S.; Yakhmi, J. Copper doped SnO<sub>2</sub> nanowires as highly sensitive H<sub>2</sub>S gas sensor. *Sens. Actuators B Chem.* **2009**, *138*, 587–590. [[CrossRef](#)]
95. Kolmakov, A.; Klenov, D.; Lilach, Y.; Stemmer, S.; Moskovits, M. Enhanced gas sensing by individual SnO<sub>2</sub> nanowires and nanobelts functionalized with Pd catalyst particles. *Nano Lett.* **2005**, *5*, 667–673. [[CrossRef](#)]
96. Castillo, C.; Cabello, G.; Chornik, B.; Huentupil, Y.; Buono-Core, G. Characterization of photochemically grown Pd loaded WO<sub>3</sub> thin films and its evaluation as ammonia gas sensor. *J. Alloys Compd.* **2020**, *825*, 154166. [[CrossRef](#)]
97. Boudiba, A.; Roussel, P.; Zhang, C.; Olivier, M.-G.; Snyders, R.; Debliquy, M. Sensing mechanism of hydrogen sensors based on palladium-loaded tungsten oxide (Pd-WO<sub>3</sub>). *Sens. Actuators B Chem.* **2013**, *187*, 84–93. [[CrossRef](#)]
98. Van Tong, P.; Hoa, N.D.; Van Duy, N.; Le, D.T.T.; Van Hieu, N. Enhancement of gas-sensing characteristics of hydrothermally synthesized WO<sub>3</sub> nanorods by surface decoration with Pd nanoparticles. *Sens. Actuators B Chem.* **2016**, *223*, 453–460. [[CrossRef](#)]
99. Liu, B.; Cai, D.; Liu, Y.; Wang, D.; Wang, L.; Wang, Y.; Li, H.; Li, Q.; Wang, T. Improved room-temperature hydrogen sensing performance of directly formed Pd/WO<sub>3</sub> nanocomposite. *Sens. Actuators B Chem.* **2014**, *193*, 28–34. [[CrossRef](#)]
100. Lee, J.; Kim, S.Y.; Yoo, H.S.; Lee, W. Pd-WO<sub>3</sub> chemiresistive sensor with reinforced self-assembly for hydrogen detection at room temperature. *Sens. Actuators B Chem.* **2022**, *368*, 132236. [[CrossRef](#)]
101. Li, B.; Zhou, Q.; Peng, S.; Liao, Y. Recent advances of SnO<sub>2</sub>-based sensors for detecting volatile organic compounds. *Front. Chem.* **2020**, *8*, 321. [[CrossRef](#)]
102. Kim, B.; Lu, Y.; Hannon, A.; Meyyappan, M.; Li, J. Low temperature Pd/SnO<sub>2</sub> sensor for carbon monoxide detection. *Sens. Actuators B Chem.* **2013**, *177*, 770–775. [[CrossRef](#)]
103. Gangwar, A.K.; Godiwal, R.; Srivastava, S.; Pal, P.; Gupta, G.; Singh, P. Preparation of nanocrystalline Pd/SnO<sub>2</sub> thin films deposited on alumina substrate by reactive magnetron sputtering for efficient CO gas sensing. *Mater. Res. Bull.* **2022**, *148*, 111692. [[CrossRef](#)]
104. Meng, X.; Bi, M.; Xiao, Q.; Gao, W. Ultra-fast response and highly selectivity hydrogen gas sensor based on Pd/SnO<sub>2</sub> nanoparticles. *Int. J. Hydrog. Energy* **2022**, *47*, 3157–3169. [[CrossRef](#)]
105. Barbosa, M.S.; Suman, P.H.; Kim, J.J.; Tuller, H.L.; Orlandi, M.O. Investigation of electronic and chemical sensitization effects promoted by Pt and Pd nanoparticles on single-crystalline SnO nanobelt-based gas sensors. *Sens. Actuators B Chem.* **2019**, *301*, 127055. [[CrossRef](#)]
106. Liu, C.; Kuang, Q.; Xie, Z.; Zheng, L. The effect of noble metal (Au, Pd and Pt) nanoparticles on the gas sensing performance of SnO<sub>2</sub>-based sensors: A case study on the (221) high-index faceted SnO<sub>2</sub> octahedra. *CrystEngComm* **2015**, *17*, 6308–6313. [[CrossRef](#)]
107. Zhu, L.-Y.; Ou, L.-X.; Mao, L.-W.; Wu, X.-Y.; Liu, Y.-P.; Lu, H.-L. Advances in Noble Metal-Decorated Metal Oxide Nanomaterials for Chemiresistive Gas Sensors: Overview. *Nano-Micro Lett.* **2023**, *15*, 89. [[CrossRef](#)] [[PubMed](#)]

108. Choi, M.S.; Mirzaei, A.; Na, H.G.; Kim, S.; Kim, D.E.; Lee, K.H.; Jin, C.; Choi, S.-W. Facile and fast decoration of SnO<sub>2</sub> nanowires with Pd embedded SnO<sub>2</sub>–x nanoparticles for selective NO<sub>2</sub> gas sensing. *Sens. Actuators B Chem.* **2021**, *340*, 129984. [[CrossRef](#)]
109. Kamal Hossain, M.; Ahmed Drmash, Q. Noble Metal-Decorated Nanostructured Zinc Oxide: Strategies to Advance Chemiresistive Hydrogen Gas Sensing. *Chem. Rec.* **2022**, *22*, e202200090. [[CrossRef](#)]
110. Wang, Y.; Meng, X.; Yao, M.; Sun, G.; Zhang, Z. Enhanced CH<sub>4</sub> sensing properties of Pd modified ZnO nanosheets. *Ceram. Int.* **2019**, *45*, 13150–13157. [[CrossRef](#)]
111. Alexiadou, M.; Kandyla, M.; Mousdis, G.; Kompitsas, M. Pulsed laser deposition of ZnO thin films decorated with Au and Pd nanoparticles with enhanced acetone sensing performance. *Appl. Phys. A* **2017**, *123*, 262. [[CrossRef](#)]
112. Jemai, R.; Djebbi, M.A.; Hussain, N.; Yang, B.; Hirtz, M.; Trouillet, V.; Rhaiem, H.B.; Amara, A.B.H. Activated porous carbon supported Pd and ZnO nanocatalysts for trace sensing of carbaryl pesticide in water and food products. *New J. Chem.* **2022**, *46*, 13880–13895. [[CrossRef](#)]
113. Majhi, S.M.; Navale, S.; Mirzaei, A.; Kim, H.W.; Kim, S.S. Strategies to Boost Chemiresistive Sensing Performance of In<sub>2</sub>O<sub>3</sub>-based Gas Sensors: An Overview. *Inorg. Chem. Front.* **2023**, *10*, 3428–3467. [[CrossRef](#)]
114. Chen, C.; Chen, W.; Liu, Q.; Liu, Y.; Xiao, G.; Chen, C.; Li, F.; Zhou, J. Electrospinning of Pd-In<sub>2</sub>O<sub>3</sub> Nanofibers for High-Performance Room Temperature Hydrogen Sensors. *ACS Appl. Nano Mater.* **2022**, *5*, 12646–12655. [[CrossRef](#)]
115. Wanekaya, A.K. Applications of nanoscale carbon-based materials in heavy metal sensing and detection. *Analyst* **2011**, *136*, 4383–4391. [[CrossRef](#)]
116. Raju, C.V.; Cho, C.H.; Rani, G.M.; Manju, V.; Umapathi, R.; Huh, Y.S.; Park, J.P. Emerging insights into the use of carbon-based nanomaterials for the electrochemical detection of heavy metal ions. *Coord. Chem. Rev.* **2023**, *476*, 214920. [[CrossRef](#)]
117. Nabgan, W.; Jalil, A.A.; Nabgan, B.; Ikram, M.; Ali, M.W.; Lakshminarayana, P. A state of the art overview of carbon-based composites applications for detecting and eliminating pharmaceuticals containing wastewater. *Chemosphere* **2022**, *288*, 132535. [[CrossRef](#)]
118. Yang, Z.; Zhang, X.; Guo, J. Functionalized Carbon-Based Electrochemical Sensors for Food and Alcoholic Beverage Safety. *Appl. Sci.* **2022**, *12*, 9082. [[CrossRef](#)]
119. Singh, P.; Kumar, S.; Kumar, P.; Kataria, N.; Bhankar, V.; Kumar, K.; Kumar, R.; Hsieh, C.-T.; Khoo, K.S. Assessment of biomass-derived carbon dots as highly sensitive and selective templates for the sensing of hazardous ions. *Nanoscale* **2023**. [[CrossRef](#)]
120. Mehdipour-Ataei, S.; Aram, E. Mesoporous Carbon-Based Materials: A Review of Synthesis, Modification, and Applications. *Catalysts* **2022**, *13*, 2. [[CrossRef](#)]
121. Adams, B.D.; Chen, A. The role of palladium in a hydrogen economy. *Mater. Today* **2011**, *14*, 282–289. [[CrossRef](#)]
122. Raseruthe, K.E.; Matthews, T.; Gwebu, S.S.; Pillay, K.; Maxakato, N.W. Investigating the effect of carbon support on palladium-based catalyst towards electro-oxidation of ethylene glycol. *Mater. Res. Express* **2021**, *8*, 015017. [[CrossRef](#)]
123. Travlou, N.A.; Seredych, M.; Rodríguez-Castellón, E.; Bandoz, T.J. Activated carbon-based gas sensors: Effects of surface features on the sensing mechanism. *J. Mater. Chem. A* **2015**, *3*, 3821–3831. [[CrossRef](#)]
124. Veeramani, V.; Sivakumar, M.; Chen, S.-M.; Madhu, R.; Alamri, H.R.; Allothman, Z.A.; Hossain, M.S.A.; Chen, C.-K.; Yamauchi, Y.; Miyamoto, N. Lignocellulosic biomass-derived, graphene sheet-like porous activated carbon for electrochemical supercapacitor and catechin sensing. *RSC Adv.* **2017**, *7*, 45668–45675. [[CrossRef](#)]
125. Xing, X.; Li, Z.; Chen, X.; Du, L.; Tian, Y.; Feng, D.; Wang, C.; Liu, G.; Yang, D. Three-dimensional porous carbon/nitrogen framework-decorated palladium nanoparticles for stable and wide-concentration-range hydrogen sensing. *ACS Appl. Mater. Interfaces* **2022**, *14*, 17911–17919. [[CrossRef](#)] [[PubMed](#)]
126. Bo, X.; Bai, J.; Ju, J.; Guo, L. A sensitive amperometric sensor for hydrazine and hydrogen peroxide based on palladium nanoparticles/onion-like mesoporous carbon vesicle. *Anal. Chim. Acta* **2010**, *675*, 29–35. [[CrossRef](#)] [[PubMed](#)]
127. Koskun, Y.; Şavk, A.; Şen, B.; Şen, F. Highly sensitive glucose sensor based on monodisperse palladium nickel/activated carbon nanocomposites. *Anal. Chim. Acta* **2018**, *1010*, 37–43. [[CrossRef](#)] [[PubMed](#)]
128. Veerakumar, P.; Veeramani, V.; Chen, S.-M.; Madhu, R.; Liu, S.-B. Palladium nanoparticle incorporated porous activated carbon: Electrochemical detection of toxic metal ions. *ACS Appl. Mater. Interfaces* **2016**, *8*, 1319–1326. [[CrossRef](#)]
129. Zhang, T.; Jin, H.; Fang, Y.; Guan, J.; Ma, S.; Pan, Y.; Zhang, M.; Zhu, H.; Liu, X.; Du, M. Detection of trace Cd<sup>2+</sup>, Pb<sup>2+</sup> and Cu<sup>2+</sup> ions via porous activated carbon supported palladium nanoparticles modified electrodes using SWASV. *Mater. Chem. Phys.* **2019**, *225*, 433–442. [[CrossRef](#)]
130. Nag, A.; Mitra, A.; Mukhopadhyay, S.C. Graphene and its sensor-based applications: A review. *Sens. Actuators A Phys.* **2018**, *270*, 177–194. [[CrossRef](#)]
131. Sainz-Urruela, C.; Vera-López, S.; San Andrés, M.P.; Díez-Pascual, A.M. Graphene-based sensors for the detection of bioactive compounds: A review. *Int. J. Mol. Sci.* **2021**, *22*, 3316. [[CrossRef](#)] [[PubMed](#)]
132. Khan, M.; Assal, M.E.; Tahir, M.N.; Khan, M.; Ashraf, M.; Hatshan, M.R.; Khan, M.; Varala, R.; Badawi, N.M.; Adil, S.F. Graphene/inorganic nanocomposites: Evolving photocatalysts for solar energy conversion for environmental remediation. *J. Saudi Chem. Soc.* **2022**, *26*, 101544. [[CrossRef](#)]
133. Palanisamy, S.; Ku, S.; Chen, S.-M. Dopamine sensor based on a glassy carbon electrode modified with a reduced graphene oxide and palladium nanoparticles composite. *Microchim. Acta* **2013**, *180*, 1037–1042. [[CrossRef](#)]
134. Jiang, J.; Du, X. Sensitive electrochemical sensors for simultaneous determination of ascorbic acid, dopamine, and uric acid based on Au@Pd-reduced graphene oxide nanocomposites. *Nanoscale* **2014**, *6*, 11303–11309. [[CrossRef](#)]

135. Wang, J.; Yang, B.; Zhang, K.; Bin, D.; Shiraiishi, Y.; Yang, P.; Du, Y. Highly sensitive electrochemical determination of Sunset Yellow based on the ultrafine Au-Pd and reduced graphene oxide nanocomposites. *J. Colloid Interface Sci.* **2016**, *481*, 229–235. [[CrossRef](#)]
136. Shin, D.H.; Kim, W.; Jun, J.; Lee, J.S.; Kim, J.H.; Jang, J. Highly selective FET-type glucose sensor based on shape-controlled palladium nanoflower-decorated graphene. *Sens. Actuators B Chem.* **2018**, *264*, 216–223. [[CrossRef](#)]
137. Fu, L.; Yu, S.; Thompson, L.; Yu, A. Development of a novel nitrite electrochemical sensor by stepwise in situ formation of palladium and reduced graphene oxide nanocomposites. *RSC Adv.* **2015**, *5*, 40111–40116. [[CrossRef](#)]
138. Yi, W.; Li, Z.; Dong, C.; Li, H.-W.; Li, J. Electrochemical detection of chloramphenicol using palladium nanoparticles decorated reduced graphene oxide. *Microchem. J.* **2019**, *148*, 774–783. [[CrossRef](#)]
139. Demirkan, B.; Bozkurt, S.; Cellat, K.; Arikan, K.; Yılmaz, M.; Şavk, A.; Çalimli, M.H.; Nas, M.S.; Atalar, M.N.; Alma, M.H. Palladium supported on polypyrrole/reduced graphene oxide nanoparticles for simultaneous biosensing application of ascorbic acid, dopamine, and uric acid. *Sci. Rep.* **2020**, *10*, 2946. [[CrossRef](#)]
140. Dong, Y.; Wang, Q.; Wu, H.; Chen, Y.; Lu, C.H.; Chi, Y.; Yang, H.H. Graphitic carbon nitride materials: Sensing, imaging and therapy. *Small* **2016**, *12*, 5376–5393. [[CrossRef](#)]
141. Xavier, M.M.; Nair, P.R.; Mathew, S. Emerging trends in sensors based on carbon nitride materials. *Analyst* **2019**, *144*, 1475–1491. [[CrossRef](#)] [[PubMed](#)]
142. Raghu, S.; Santhosh, P.; Ramaprabhu, S. Nanostructured palladium modified graphitic carbon nitride-high performance room temperature hydrogen sensor. *Int. J. Hydrogen Energy* **2016**, *41*, 20779–20786.
143. Tarditi, A.M.; Cornaglia, L.M. Novel PdAgCu ternary alloy as promising materials for hydrogen separation membranes: Synthesis and characterization. *Surf. Sci.* **2011**, *605*, 62–71. [[CrossRef](#)]
144. Wang, L.; An, F.; Liu, X.; Zhang, D.; Yang, Z. Preparation and Hydrogen-Sensitive Property of WO<sub>3</sub>/Graphene/Pd Ternary Composite. *Chemosensors* **2023**, *11*, 410. [[CrossRef](#)]
145. Wang, D.; Zhang, D.; Mi, Q. A high-performance room temperature benzene gas sensor based on CoTiO<sub>3</sub> covered TiO<sub>2</sub> nanospheres decorated with Pd nanoparticles. *Sens. Actuators B Chem.* **2022**, *350*, 130830. [[CrossRef](#)]
146. Turunc, E. Synthesis, characterization and sensing application of HNTs@ Pd-MoS<sub>2</sub> ternary composite. *Mater. Today Commun.* **2022**, *31*, 103555. [[CrossRef](#)]
147. Bai, H.; Guo, H.; Feng, C.; Wang, J.; Liu, B.; Xie, Z.; Guo, F.; Chen, D.; Zhang, R.; Zheng, Y. Highly responsive and selective ppb-level NO<sub>2</sub> gas sensor based on porous Pd-functionalized CuO/rGO at room temperature. *J. Mater. Chem. C* **2022**, *10*, 3756–3769. [[CrossRef](#)]
148. Ghosal, S.; Bhattacharyya, P. A review on the sensing performances for three different ternary hybrid (Pd/RGO/TiO<sub>2</sub>-NTs, Pd/RGO/MnO<sub>2</sub>-NFs and Pd/RGO/WO<sub>3</sub>-NFs) gas sensor device structures. *CSI Trans. ICT* **2020**, *8*, 117–122. [[CrossRef](#)]
149. Luo, S.; Chen, R.; Wang, J.; Xiang, L. Conductometric methane gas sensors based on ZnO/Pd@ ZIF-8: Effect of dual filtering of ZIF-8 to increase the selectivity. *Sens. Actuators B Chem.* **2023**, *383*, 133600. [[CrossRef](#)]
150. Salman, F.; Kazici, H.C.; Kivrak, H. Electrochemical sensor investigation of carbon-supported PdCoAg multimetal catalysts using sugar-containing beverages. *Front. Chem. Sci. Eng.* **2020**, *14*, 629–638. [[CrossRef](#)]
151. El-Nowihy, G.H.; El-Deab, M.S. Tailor-designed Pd-Cu-Ni/rGO nanocomposite for efficient glucose electro-oxidation. *J. Electroanal. Chem.* **2022**, *925*, 116917. [[CrossRef](#)]
152. Zhang, C.; Ren, J.; Xing, Y.; Cui, M.; Li, N.; Liu, P.; Wen, X.; Li, M. Fabrication of hollow ZnO-Co<sub>3</sub>O<sub>4</sub> nanocomposite derived from bimetallic-organic frameworks capped with Pd nanoparticles and MWCNTs for highly sensitive detection of tanshinol drug. *Mater. Sci. Eng. C* **2020**, *108*, 110214. [[CrossRef](#)] [[PubMed](#)]
153. Zhao, C.; Zhou, J.; Yan, Y.; Yang, L.; Xing, G.; Li, H.; Wu, P.; Wang, M.; Zheng, H. Application of coagulation/flocculation in oily wastewater treatment: A review. *Sci. Total Environ.* **2021**, *765*, 142795. [[CrossRef](#)] [[PubMed](#)]
154. Pasinszki, T.; Krebsz, M. Synthesis and application of zero-valent iron nanoparticles in water treatment, environmental remediation, catalysis, and their biological effects. *Nanomaterials* **2020**, *10*, 917. [[CrossRef](#)]
155. Samaei, S.M.; Gato-Trinidad, S.; Altaee, A. Performance evaluation of reverse osmosis process in the post-treatment of mining wastewaters: Case study of Costerfield mining operations, Victoria, Australia. *J. Water Process Eng.* **2020**, *34*, 101116. [[CrossRef](#)]
156. Behera, A.; Mansingh, S.; Das, K.K.; Parida, K. Synergistic ZnFe<sub>2</sub>O<sub>4</sub>-carbon allotropes nanocomposite photocatalyst for norfloxacin degradation and Cr (VI) reduction. *J. Colloid Interface Sci.* **2019**, *544*, 96–111. [[CrossRef](#)]
157. Li, X.; Yi, K.; Ran, Q.; Fan, Z.; Liu, C.; Liu, X.; Jia, K. Selective removal of cationic organic dyes via electrospun nanofibrous membranes derived from polyarylene ethers containing pendent nitriles and sulfonates. *Sep. Purif. Technol.* **2022**, *301*, 121942. [[CrossRef](#)]
158. Feng, Y.; Yin, J.; Liu, S.; Wang, Y.; Li, B.; Jiao, T. Facile synthesis of Ag/Pd nanoparticle-loaded poly (ethylene imine) composite hydrogels with highly efficient catalytic reduction of 4-nitrophenol. *ACS Omega* **2020**, *5*, 3725–3733. [[CrossRef](#)] [[PubMed](#)]
159. Zhang, Z.; Sun, T.; Chen, C.; Xiao, F.; Gong, Z.; Wang, S. Bifunctional nanocatalyst based on three-dimensional carbon nanotube-graphene hydrogel supported Pd nanoparticles: One-pot synthesis and its catalytic properties. *ACS Appl. Mater. Interfaces* **2014**, *6*, 21035–21040. [[CrossRef](#)]
160. Kalantari, E.; Khalilzadeh, M.A.; Zareyee, D. Effective Reduction of Cr (VI) and Organic Dyes Using Pd NPs/Fe<sub>3</sub>O<sub>4</sub>@ nanocellulose as a Recoverable Catalyst in Aqueous Media. *J. Inorg. Organomet. Polym. Mater.* **2021**, *31*, 319–330. [[CrossRef](#)]

161. Zhang, Y.; Park, S.-J. Stabilization of dispersed CuPd bimetallic alloy nanoparticles on ZIF-8 for photoreduction of Cr (VI) in aqueous solution. *Chem. Eng. J.* **2019**, *369*, 353–362. [[CrossRef](#)]
162. Ge, L.; Zhang, M.; Wang, R.; Li, N.; Zhang, L.; Liu, S.; Jiao, T. Fabrication of CS/GA/RGO/Pd composite hydrogels for highly efficient catalytic reduction of organic pollutants. *RSC Adv.* **2020**, *10*, 15091–15097. [[CrossRef](#)] [[PubMed](#)]
163. Yang, W.; Pan, M.; Huang, C.; Zhao, Z.; Wang, J.; Zeng, H. Graphene oxide-based noble-metal nanoparticles composites for environmental application. *Compos. Commun.* **2021**, *24*, 100645. [[CrossRef](#)]
164. Dadashi, J.; Ghasemzadeh, M.A.; Salavati-Niasari, M. Recent developments in hydrogels containing copper and palladium for the catalytic reduction/degradation of organic pollutants. *RSC Adv.* **2022**, *12*, 23481–23502. [[CrossRef](#)]
165. Omole, M.A.; K'Owino, I.O.; Sadik, O.A. Palladium nanoparticles for catalytic reduction of Cr (VI) using formic acid. *Appl. Catal. B: Environ.* **2007**, *76*, 158–167. [[CrossRef](#)]
166. Bao, S.; Liu, H.; Liu, Y.; Yang, W.; Wang, Y.; Yu, Y.; Sun, Y.; Li, K. Amino-functionalized graphene oxide-supported networked Pd–Ag nanowires as highly efficient catalyst for reducing Cr (VI) in industrial effluent by formic acid. *Chemosphere* **2020**, *257*, 127245. [[CrossRef](#)]
167. Besharat, F.; Ahmadpoor, F.; Nasrollahzadeh, M. Graphene-based (nano) catalysts for the reduction of Cr (VI): A review. *J. Mol. Liq.* **2021**, *334*, 116123. [[CrossRef](#)]
168. Cherifi, Y.; Barras, A.; Addad, A.; Ouddane, B.; Roussel, P.; Chaouchi, A.; Szunerits, S.; Boukherroub, R. Simultaneous photocatalytic Cr (VI) reduction and phenol degradation over copper sulphide-reduced graphene oxide nanocomposite under visible light irradiation: Performance and reaction mechanism. *Chemosphere* **2021**, *268*, 128798. [[CrossRef](#)]
169. Iqbal, M.; Kaneti, Y.V.; Kim, J.; Yulianto, B.; Kang, Y.M.; Bando, Y.; Sugahara, Y.; Yamauchi, Y. Chemical design of palladium-based nanoarchitectures for catalytic applications. *Small* **2019**, *15*, 1804378. [[CrossRef](#)]
170. Simon, A.; Mathai, S. Recent Advances in Heterogeneous Magnetic Pd-NHC Catalysts in Organic Transformations. *J. Organomet. Chem.* **2023**, *996*, 122768. [[CrossRef](#)]
171. Baran, T.; Nasrollahzadeh, M. Facile synthesis of palladium nanoparticles immobilized on magnetic biodegradable microcapsules used as effective and recyclable catalyst in Suzuki-Miyaura reaction and p-nitrophenol reduction. *Carbohydr. Polym.* **2019**, *222*, 115029. [[CrossRef](#)] [[PubMed](#)]
172. Senthilkumar, M.; Manisankar, P.; Pandimurugan, R.; Vivekanand, P.; Periyasami, G.; Harikumar, S.; Karthikeyan, P.; Rahaman, M.; Khanal, S. Nano-Pd/Chitosan Composite: An Extremely Effective Catalyst to the Synthesis of Pyrazolyl Analogues through Suzuki-Miyaura Cross-Coupling Reactions in an Aqueous Medium. *J. Chem.* **2023**, *2023*, 6594464. [[CrossRef](#)]
173. Eswaran, M.; Dhanusuraman, R.; Tsai, P.-C.; Ponnusamy, V.K. One-step preparation of graphitic carbon nitride/Polyaniline/Palladium nanoparticles based nanohybrid composite modified electrode for efficient methanol electro-oxidation. *Fuel* **2019**, *251*, 91–97. [[CrossRef](#)]
174. Jose, J.; Jose, S.P.; Prasankumar, T.; Shaji, S.; Pillai, S. Emerging ternary nanocomposite of rGO draped palladium oxide/polypyrrole for high performance supercapacitors. *J. Alloys Compd.* **2021**, *855*, 157481. [[CrossRef](#)]
175. Fuku, K.; Takioka, R.; Iwamura, K.; Todoroki, M.; Sayama, K.; Ikenaga, N. Photocatalytic H<sub>2</sub>O<sub>2</sub> production from O<sub>2</sub> under visible light irradiation over phosphate ion-coated Pd nanoparticles-supported BiVO<sub>4</sub>. *Appl. Catal. B Environ.* **2020**, *272*, 119003. [[CrossRef](#)]
176. Heravi, M.M.; Asadi, S.; Hoseini Chopani, S.M.; Jaderi, E. N-Heterocyclic Carbene-Palladium Complex onto Graphene Oxide and Poly (ethylene glycol)(PEG) Applied as Superior Catalyst for the Suzuki-Miyaura Cross-Coupling Reaction in Water. *Appl. Organomet. Chem.* **2020**, *34*, e5805. [[CrossRef](#)]
177. Ault, A. The Nobel prize in chemistry for 2001. *J. Chem. Educ.* **2002**, *79*, 572. [[CrossRef](#)]
178. Biffis, A.; Centomo, P.; Del Zotto, A.; Zecca, M. Pd metal catalysts for cross-couplings and related reactions in the 21st century: A critical review. *Chem. Rev.* **2018**, *118*, 2249–2295. [[CrossRef](#)]
179. Ameen, I.; Iqbal, S.; Hussain, M.; Alothman, A.A.; Algahtani, H.A.; Mushab, M.S.S.; Iqbal, A.; Perveen, S.; Musaddiq, S. Ag, Au and ZrO<sub>2</sub>@ reduced graphene oxide nanocomposites; Pd free catalysis of suzuki-miyaura coupling reactions. *Mater. Res. Express* **2023**, *10*, 045102. [[CrossRef](#)]
180. Kyomuhimbo, H.D.; Feleni, U. Electroconductive Green Metal-polyaniline Nanocomposites: Synthesis and Application in Sensors. *Electroanalysis* **2023**, *35*, e202100636. [[CrossRef](#)]
181. Nayak, S.; Kittur, A.; Nayak, S.; Murgunde, B. Binderless nano marigold flower like structure of nickel sulfide electrode for sustainable supercapacitor energy storage applications. *J. Energy Storage* **2023**, *62*, 106963. [[CrossRef](#)]
182. Zhao, X.; Chang, Y.; Chen, W.-J.; Wu, Q.; Pan, X.; Chen, K.; Weng, B. Recent progress in Pd-based nanocatalysts for selective hydrogenation. *ACS Omega* **2021**, *7*, 17–31. [[CrossRef](#)] [[PubMed](#)]
183. Zhong, Y.; Mao, Y.; Shi, S.; Wan, M.; Ma, C.; Wang, S.; Chen, C.; Zhao, D.; Zhang, N. Fabrication of magnetic Pd/MOF hollow nanospheres with double-shell structure: Toward highly efficient and recyclable nanocatalysts for hydrogenation reaction. *ACS Appl. Mater. Interfaces* **2019**, *11*, 32251–32260. [[CrossRef](#)] [[PubMed](#)]
184. Shakil Hussain, S.; Kamal, M.S.; Hossain, M.K. Recent developments in nanostructured palladium and other metal catalysts for organic transformation. *J. Nanomater.* **2019**, *2019*, 1562130. [[CrossRef](#)]
185. Advani, J.H.; Noor-ul, H.K.; Bajaj, H.C.; Biradar, A.V. Stabilization of palladium nanoparticles on chitosan derived N-doped carbon for hydrogenation of various functional groups. *Appl. Surf. Sci.* **2019**, *487*, 1307–1315. [[CrossRef](#)]

186. Pisarenko, E.; Ponomarev, A.; Pisarenko, V. Studying the selective methylacetylene hydrogenation reaction in methylacetylene-propylene mixtures on palladium oxide nanocatalysts. *Theor. Found. Chem. Eng.* **2021**, *55*, 380–389. [[CrossRef](#)]
187. Liang, Y.; Das, U.K.; Luo, J.; Diskin-Posner, Y.; Avram, L.; Milstein, D. Magnesium Pincer Complexes and Their Applications in Catalytic Semihydrogenation of Alkynes and Hydrogenation of Alkenes: Evidence for Metal-Ligand Cooperation. *J. Am. Chem. Soc.* **2022**, *144*, 19115–19126. [[CrossRef](#)]
188. Lv, H.; Qin, H.; Sun, M.; Jia, F.; Huang, B.; Liu, B. Mesoporosity-Enabled Selectivity of Mesoporous Palladium-Based Nanocrystals Catalysts in Semihydrogenation of Alkynes. *Angew. Chem.* **2022**, *134*, e202114539. [[CrossRef](#)]
189. Gulbagca, F.; Aygün, A.; Gülcan, M.; Ozdemir, S.; Gonca, S.; Şen, F. Green synthesis of palladium nanoparticles: Preparation, characterization, and investigation of antioxidant, antimicrobial, anticancer, and DNA cleavage activities. *Appl. Organomet. Chem.* **2021**, *35*, e6272. [[CrossRef](#)]
190. Chen, Y.; Chen, Z.; Yang, D.; Zhu, L.; Liang, Z.; Pang, Y.; Zhou, L. Novel Microbial Palladium Nanoparticles with a High Photothermal Effect for Antibacterial Applications. *ACS Omega* **2022**, *8*, 1534–1541. [[CrossRef](#)]
191. Liu, J.; Wang, L.; Shen, X.; Gao, X.; Chen, Y.; Liu, H.; Liu, Y.; Yin, D.; Liu, Y.; Xu, W. Graphdiyne-templated palladium-nanoparticle assembly as a robust oxygen generator to attenuate tumor hypoxia. *Nano Today* **2020**, *34*, 100907. [[CrossRef](#)]
192. Ramalingam, V.; Raja, S.; Harshavardhan, M. In situ one-step synthesis of polymer-functionalized palladium nanoparticles: An efficient anticancer agent against breast cancer. *Dalton Trans.* **2020**, *49*, 3510–3518. [[CrossRef](#)]
193. MubarakAli, D.; Kim, H.; Venkatesh, P.S.; Kim, J.-W.; Lee, S.-Y. A systemic review on the synthesis, characterization, and applications of palladium nanoparticles in biomedicine. *Appl. Biochem. Biotechnol.* **2023**, *195*, 3699–3718. [[CrossRef](#)]
194. Luo, S.; Liu, Y.; Zhu, Y.; Niu, Q.; Cheng, M.; Ye, S.; Yi, H.; Shao, B.; Shen, M.; Wen, X. Perspectives on palladium-based nanomaterials: Green synthesis, ecotoxicity, and risk assessment. *Environ. Sci. Nano* **2021**, *8*, 20–36. [[CrossRef](#)]
195. Subhan, A.; Mourad, A.-H.I.; Al-Douri, Y. Influence of laser process parameters, liquid medium, and external field on the synthesis of colloidal metal nanoparticles using pulsed laser ablation in liquid: A review. *Nanomaterials* **2022**, *12*, 2144. [[CrossRef](#)] [[PubMed](#)]
196. Salman, S.H.; Khashan, K.S.; Hadi, A.A. Green Synthesis and Characterization of Palladium Nanoparticles by Pulsed Laser Ablation and Their Antibacterial Activity. *Metals* **2023**, *13*, 273. [[CrossRef](#)]
197. Liu, Y.; Li, J.; Chen, M.; Chen, X.; Zheng, N. Palladium-based nanomaterials for cancer imaging and therapy. *Theranostics* **2020**, *10*, 10057. [[CrossRef](#)]
198. Mari, E.; Tsai, P.-C.; Eswaran, M.; Ponnusamy, V.K. Efficient electro-catalytic oxidation of ethylene glycol using flower-like graphitic carbon nitride/iron oxide/palladium nanocomposite for fuel cell application. *Fuel* **2020**, *280*, 118646. [[CrossRef](#)]
199. Rahman, M.U.; Xie, F.; Sun, X.; Wei, M. Palladium nanoparticles on nitrogen doped acetylene carbon black as an efficient counter electrode for dye-sensitized solar cells. *J. Electroanal. Chem.* **2019**, *848*, 113317. [[CrossRef](#)]
200. Vinayan, B.; Sethupathi, K.; Ramaprabhu, S. Facile synthesis of triangular shaped palladium nanoparticles decorated nitrogen doped graphene and their catalytic study for renewable energy applications. *Int. J. Hydrogen Energy* **2013**, *38*, 2240–2250. [[CrossRef](#)]
201. Dal Pont, K.; Serghei, A.; Espuche, E. Multifunctional Pd-Based Nanocomposites with Designed Structure from In Situ Growth of Pd Nanoparticles and Polyether Block Amide Copolymer. *Polymers* **2021**, *13*, 1477. [[CrossRef](#)] [[PubMed](#)]
202. Oliveira, A.; Silva, S.; Rubinger, C.; Ider, J.; Rubinger, R.; Oliveira, E.; Doriguetto, A.; de Carvalho, H. Preparation and characterization of palladium-doped titanium dioxide for solar cell applications. *Mater. Sci. Eng. B* **2022**, *280*, 115702. [[CrossRef](#)]
203. Slavcheva, E.; Ganske, G.; Schnakenberg, U. Sputtered Pd as hydrogen storage for a chip-integrated microenergy system. *Sci. World J.* **2014**, *2014*, 146126. [[CrossRef](#)] [[PubMed](#)]
204. Alexeeva, O.; Fateev, V. Application of the magnetron sputtering for nanostructured electrocatalysts synthesis. *Int. J. Hydrogen Energy* **2016**, *41*, 3373–3386. [[CrossRef](#)]
205. Mendivil, M.; Krishnan, B.; Castillo, G.; Shaji, S. Synthesis and properties of palladium nanoparticles by pulsed laser ablation in liquid. *Appl. Surf. Sci.* **2015**, *348*, 45–53. [[CrossRef](#)]
206. Marzun, G.; Nakamura, J.; Zhang, X.; Barcikowski, S.; Wagener, P. Size control and supporting of palladium nanoparticles made by laser ablation in saline solution as a facile route to heterogeneous catalysts. *Appl. Surf. Sci.* **2015**, *348*, 75–84. [[CrossRef](#)]
207. Pan, W.; Zhang, X.; Ma, H.; Zhang, J. Electrochemical synthesis, voltammetric behavior, and electrocatalytic activity of Pd nanoparticles. *J. Phys. Chem. C* **2008**, *112*, 2456–2461. [[CrossRef](#)]
208. Okitsu, K.; Yue, A.; Tanabe, S.; Matsumoto, H. Sonochemical preparation and catalytic behavior of highly dispersed palladium nanoparticles on alumina. *Chem. Mater.* **2000**, *12*, 3006–3011. [[CrossRef](#)]
209. Qiu, X.-F.; Xu, J.-Z.; Zhu, J.-M.; Zhu, J.-J.; Xu, S.; Chen, H.-Y. Controllable synthesis of palladium nanoparticles via a simple sonoelectrochemical method. *J. Mater. Res.* **2003**, *18*, 1399–1404. [[CrossRef](#)]
210. Nemamcha, A.; Rehspringer, J.-L.; Khatmi, D. Synthesis of palladium nanoparticles by sonochemical reduction of palladium (II) nitrate in aqueous solution. *J. Phys. Chem. B* **2006**, *110*, 383–387. [[CrossRef](#)]
211. Jiang, R.; Zhang, Y.; Swier, S.; Wei, X.; Erkey, C.; Kunz, H.R.; Fenton, J.M. Preparation via supercritical fluid route of Pd-impregnated nafion membranes which exhibit reduced methanol crossover for DMFC. *Electrochem. Solid-State Lett.* **2005**, *8*, A611. [[CrossRef](#)]
212. Moisan, S.; Marty, J.-D.; Cansell, F.; Aymonier, C. Preparation of functional hybrid palladium nanoparticles using supercritical fluids: A novel approach to detach the growth and functionalization steps. *Chem. Commun.* **2008**, 1428–1430. [[CrossRef](#)] [[PubMed](#)]

213. Cansell, F.; Aymonier, C. Design of functional nanostructured materials using supercritical fluids. *J. Supercrit. Fluids* **2009**, *47*, 508–516. [[CrossRef](#)]
214. Shanthi, K.; Sreevani, V.; Vimala, K.; Kannan, S. Cytotoxic Effect of Palladium Nanoparticles Synthesized From *Syzygium aromaticum* Aqueous Extracts and Induction of Apoptosis in Cervical Carcinoma. *Proc. Natl. Acad. Sci. India Sect. B Biol. Sci.* **2017**, *87*, 1101–1112. [[CrossRef](#)]
215. Sharmila, G.; Farzana Fathima, M.; Haries, S.; Geetha, S.; Manoj Kumar, N.; Muthukumaran, C. Green synthesis, characterization and antibacterial efficacy of palladium nanoparticles synthesized using *Filicium decipiens* leaf extract. *J. Mol. Struct.* **2017**, *1138*, 35–40. [[CrossRef](#)]
216. Sharmila, G.; Haries, S.; Farzana Fathima, M.; Geetha, S.; Manoj Kumar, N.; Muthukumaran, C. Enhanced catalytic and antibacterial activities of phytosynthesized palladium nanoparticles using *Santalum album* leaf extract. *Powder Technol.* **2017**, *320*, 22–26. [[CrossRef](#)]
217. Shaik, M.R.; Ali, Z.J.Q.; Khan, M.; Kuniyil, M.; Assal, M.E.; Alkathlan, H.Z.; Al-Warthan, A.; Siddiqui, M.R.H.; Khan, M.; Adil, S.F. Green Synthesis and Characterization of Palladium Nanoparticles Using *Origanum vulgare* L. Extract and Their Catalytic Activity. *Molecules* **2017**, *22*, 165. [[CrossRef](#)] [[PubMed](#)]
218. Sheny, D.S.; Philip, D.; Mathew, J. Rapid green synthesis of palladium nanoparticles using the dried leaf of *Anacardium occidentale*. *Spectrochim. Acta Part A Mol. Biomol. Spectrosc.* **2012**, *91*, 35–38. [[CrossRef](#)]
219. Anju, A.; Gupta, K.; Chundawat, T.S. In vitro antimicrobial and antioxidant activity of biogenically synthesized palladium and platinum nanoparticles using *Botryococcus braunii*. *Turk. J. Pharm. Sci.* **2020**, *17*, 299.
220. Sriramulu, M.; Sumathi, S. Biosynthesis of palladium nanoparticles using *Saccharomyces cerevisiae* extract and its photocatalytic degradation behaviour. *Adv. Nat. Sci. Nanosci. Nanotechnol.* **2018**, *9*, 025018. [[CrossRef](#)]
221. Omajali, J.B.; Gomez-Bolivar, J.; Mikheenko, I.P.; Sharma, S.; Kayode, B.; Al-Duri, B.; Banerjee, D.; Walker, M.; Merroun, M.L.; Macaskie, L.E. Novel catalytically active Pd/Ru bimetallic nanoparticles synthesized by *Bacillus benzeovorans*. *Sci. Rep.* **2019**, *9*, 4715.
222. Sonbol, H.; Ameen, F.; AlYahya, S.; Almansob, A.; Alwakeel, S. Padina boryana mediated green synthesis of crystalline palladium nanoparticles as potential nanodrug against multidrug resistant bacteria and cancer cells. *Sci. Rep.* **2021**, *11*, 5444.

**Disclaimer/Publisher's Note:** The statements, opinions and data contained in all publications are solely those of the individual author(s) and contributor(s) and not of MDPI and/or the editor(s). MDPI and/or the editor(s) disclaim responsibility for any injury to people or property resulting from any ideas, methods, instructions or products referred to in the content.